

DOE/ET/51013-139

UC20A

**Implications of RF Current Drive Theory
for Next Step Steady-state Tokamak Design**

by Joel H. Schultz

M.I.T. Plasma Fusion Center Report PFC/RR-85-2

June, 1985

**Implications of RF Current Drive Theory
for Next Step Steady-state Tokamak Design**

by Joel H. Schultz

M.I.T. Plasma Fusion Center Report PFC/RR-85-2

June, 1985

1.0 Introduction

Two missions have been identified for a next-step tokamak experiment in the United States. The more ambitious Mission II device would be a superconducting tokamak, capable of doing long-pulse ignition demonstrations, and hopefully capable of also being able to achieve steady-state burn. A few interesting lines of approach have been identified, using a combination of logical design criteria and parametric system scans [SC85]. These include:

- 1 TIBER: A point-design suggested by Lawrence Livermore, that proposes a machine with the capability of demonstrating ignition, high beta (10 %) and high Q ($= 10$), using high frequency, fast-wave current drive. The TIBER topology uses moderate aspect ratio and high triangularity to achieve high beta.
- 2 JET Scale-up: Since JET is currently the world's highest-performance tokamak and may remain so for some time, a scale-up of JET might have many attractions, not the least of which would be the extensive data base to be developed by JET and the similarly shaped ASDEX and Big Dee. We discuss below a 5 MA plasma with the dimensions of JET. This simulation could be considered to be either a preliminary feasibility experiment on JET with a limited pulse length or a minimum performance Mission II device that duplicates the performance of JET with superconducting TF magnets in a steady-state plasma. (A 1984 study of the Toroidal Fusion Core Experiment (TFCX) by the author and E.S. Bobrov indicated that duplication of the JET plasma, using shielded superconducting TF coils but no central solenoid, was feasible.)
- 3 Magic5: It is argued here that an aspect ratio of 5 is a magic number for a good steady-state current drive experiment. A moderately-sized machine that achieves ignition and is capable of high Q , using either fast wave or slow wave current drive is described.
- 4 ET-II: The concept of a highly elongated tokamak (ET) was first proposed as a low-cost approach to Mission I, because of the possibility of achieving ohmic ignition with low-stress copper magnets. We propose that its best application is really for commercial tokamaks, using fast-wave current drive, and suggest a Mission II experiment that would be prototypical of such a reactor.

In order to evaluate the machines that were suggested by parametric scans, we have written a

code that analyzes the implications of simple current drive theory, as elucidated by Perkins [PE83], Fisch [FI81], Karney [KA84] and Rutherford [RU81], by scanning plasmas at the pressure limit of each of the four tokamaks described above over a range of densities and temperatures. It is frequently stated, but seldom demonstrated, that the optimum temperature for reactor operation is more or less known. For an experimental machine with continuous trade-offs in efficiency, fusion power, current-drive power and credibility, the sort of scan shown below gives additional insight into the selection of the design operating temperature. The design criteria for the selection of the launched parallel index of refraction for fast-wave current drive also requires more study. Different design criteria that have been suggested include selecting n_{\parallel} equal to the accessibility limit, three times the thermal velocity, capable of carrying the plasma current in a Maxwellian tail, and capable of single-pass absorption. The implications of all four of these design criteria are examined below.

1.1 Method

Global parameters, not directly related to current drive theory are evaluated, in order to evaluate the current drive quality and power for specific designs. These are the same equations described in another study by the author [SC85], and are repeated here for ease of reference.

$$A_{surf} = \frac{P_f}{1.25P_w} \quad (1)$$

$$a = \sqrt{\frac{A_{surf}}{2\pi^2 (1 + \kappa) A}} \quad (2)$$

where A_{surf} is the plasma surface area (m^2), P_f is the fusion power (MW), P_w is the wall loading (MW/ m^2) (actually the average neutron flux through the plasma surface), κ is the plasma elongation, and A the plasma aspect ratio.

The Troyon beta limit in the first critical beta regime is expressed as:

$$\langle \beta_t \rangle = 0.033 \frac{I_p}{aB_t}$$

where β_t is the volume averaged toroidal beta, I_p is the plasma current (MA), a is the minor radius (m), and B_t is the toroidal field on axis (T).

The volume averaged specific fusion power of the plasma (W/m^3) is:

$$\frac{P_f}{V_p} = 1.33 \times 10^6 \beta_t^2 B_t^4$$

Two different correlations were used for the plasma current. One has to be used for sizing, the other as a check. The use of multiple correlations is particularly important when we explore regimes such as highly shaped plasmas in which simple analytical expressions might be expected to break down. Peng's correlation for the current was used for highly elongated plasmas, because it has the qualitatively correct feature of increasing with the square of the elongation at high elongations. My own correlation was used for moderate elongations, since Peng's correlation has no corrections for triangularity or pressure.

Peng's correlation, taking into account the detailed variation of current with inverse aspect ratio is:

$$I_p = 5 \frac{aB_t}{q_{lim}} (1.22 - 0.68\epsilon) \frac{\epsilon}{(1 - \epsilon^2)^2} \left(0.5 + \frac{\kappa^2}{2}\right)$$

where plasma current is given in MA and ϵ is the inverse aspect ratio. My correlation, also in MA, is:

$$p_{norm} = \frac{\beta_t q_{lim}^2}{\epsilon \kappa}$$

$$I_p = 8.54 B_t R_o \epsilon^{2.27} \kappa^{1.406} (1 - \Delta)^{0.39} p_{norm}^{0.0167} q_{lim}^{-1.024}$$

where p_{norm} is a normalized pressure factor to model the second order rise in current with increased plasma pressure, and Δ is the plasma triangularity.

1.1.1 Fast Wave Efficiency Modeling

The purpose of the code is to gain insight, for a given tokamak, into the way to design a fast wave launching system. The principal questions are the selection of a launching frequency, parallel index of refraction and a reference value of plasma temperature at fixed pressure. The trade-offs are perceived as follows. High temperature allows higher Q, but less fusion power above the optimum temperature. Low parallel index of refraction gives a higher theoretical current drive efficiency, but a weaker absorption. Low indices of refraction compete worse with alpha particle absorption of the wave. There are also two logical design breakpoints of interest. It may be necessary for the parallel index of refraction to be sufficiently high that there is an adequate electron tail population in a Maxwellian to carry the design current. A second criterion is that it may be necessary to design for single pass absorption, in order to avoid randomizing of the index of refraction on reflection. This criterion is generally more limiting on the minimum index of refraction than the criterion of being able to carry the current with an electron tail. A rough rule of thumb that is sometimes used to

determine the index of refraction is to keep the parallel velocity equal to three times the electron thermal velocity. The implications of these four strategies are explored in this paper. The selection of the frequency is limited to two basic options. A high frequency fast wave should be sufficiently low frequency that accessibility limits don't dominate, but otherwise as high as possible, to minimize interaction with high ion harmonics. A low frequency fast wave should be designed to equal $2.5 \omega_{c,D}$, the deuterium cyclotron frequency, in order to guarantee that the wave will not interact with any of the harmonics of deuterium, tritium or alpha particles, so long as the plasma has an aspect ratio of 5 or greater. Intermediate frequencies are expected to interact strongly with ion harmonics and are not considered. The low frequency wave has higher theoretical efficiency, because of the absence of competing absorption mechanisms. However, it is much less strongly absorbed than the high frequency wave, making single pass absorption require higher parallel indices of refraction for many plasmas, and increasing the probability of wall absorption or phase randomization by reflection. Also, a straightforward waveguide launching grill requires much more port space than for the high frequency wave, requiring cleverer launching structures, which may have more difficulty in coupling or keeping insulators clear of the fusion plasma.

In order to examine these trade-offs, a scan was made over a range of possible operating temperatures, at constant pressure and current. Within the density scan, a scan was made of all possible parallel indices of refraction. Having made the scan, four selections were made for the purposes of plotting. At each density, we looked at the index of refraction that would be (1) 1.1 times the minimum n_{\parallel} for accessibility, (2) three times the electron thermal velocity, (3) the minimum n_{\parallel} that allowed the electron tail population to carry the plasma current and (4) the minimum n_{\parallel} needed for single pass absorption.

For the density scan at constant pressure, the same profiles were assumed as in previous reactor studies [RU82] [SC85]:

$$n = n_o \left(1 - \frac{r^2}{a^2}\right)^{\frac{1}{4}}$$

$$T = T_o \left(1 - \frac{r^2}{a^2}\right)^{\frac{3}{2}}$$

This assumption gives the average ion density (10^{20} m^{-3}), as a function of average beta as:

$$n_{i,20} = \frac{B_5^2 \langle \beta \rangle_5}{T_{i,10}}$$

where B_5 is the toroidal flux density, normalized to 5 T, $\langle \beta \rangle_5$ is the average toroidal beta, normalized to 5 %, and $T_{i,10}$ is the density-weighted average ion temperature, normalized to 10 keV. With these assumptions, the specific fusion power density of the plasma (MW/m³) is:

$$P_{dt} = 2.6 n_{i,20}^2 \ln \frac{1 + 0.63 T_{i,10}^{3.5}}{T_{i,10}}$$

1.1.2 Accessibility

In order to assess accessibility, it is necessary to find the layer at which the lower hybrid frequency would equal the launching frequency. The lower hybrid frequency is a function of the dielectric constant, the square of the ratio of the electron plasma frequency to the cyclotron frequency, which can also be expressed as [RU82]:

$$\eta = 0.63 \frac{\sqrt{n_{i,20}}}{B_5}$$

where the central lower hybrid frequency (Gradians/s) is:

$$\omega_{lh,o} = 1.3 \frac{\sqrt{n_{i,20}}}{\sqrt{1 + \eta^2}}$$

For the high frequency option, a launching frequency is selected that is a fixed fraction of the central lower hybrid frequency. These studies used a launching frequency equal to half the central lower hybrid frequency, which guarantees that low parallel index of refraction waves will have good accessibility to the plasma. For the low frequency option, a launching frequency is selected that is 2.5 times the deuterium cyclotron frequency at the plasma axis. Within the selected average density, an iteration is done to find the density layer at which the plasma lower hybrid frequency equals the launched wave frequency:

$$\omega = \sqrt{\omega_{pe}^2 \left(1 - \frac{\omega_{pe}^2}{\Omega_{ce}^2}\right)}$$

The minimum accessible value of the parallel index of refraction is then:

$$n_{\parallel,min} = 1 + \frac{\omega_{pe}^2}{\Omega_{ce}^2}$$

at that layer. A well-controlled launcher might be able to launch a wave with an average parallel index of refraction of 1.1 $n_{\parallel,min}$. This is the first design option studied. The second design option sets the parallel index of refraction to three times the electron thermal velocity, or:

$$n_{\parallel} = \frac{c}{3v_{Te}}$$

where c is the speed of light, 3×10^8 (m/s), and v_{Te} is the parallel thermal velocity:

$$v_{Te} = \sqrt{\frac{kT_e}{m_e}}$$

where T_e is the electron temperature (eV), m_e is the mass of an electron, 9.1×10^{-31} (kg), and k is Boltzmann's constant, 1.6×10^{-19} (J/eV).

The purpose of selecting a wave velocity equal to three times the thermal velocity is to ensure that there will be an adequate electron population in the tail to drive the plasma current. A simple expression for the maximum current density carried by a near Maxwellian could also be used to give a more direct design criterion:

$$J_{max} = \frac{n_e e}{\sqrt{2\pi}} v_{Te} \exp \epsilon$$

where n_e is the average electron density (m^{-3}), $e = 1.6 \times 10^{-19}$ (C) is the charge on an electron, v_{Te} is the electron thermal velocity (m/s), and ϵ is the ratio of inertial to resonant electron thermal energy ():

$$\epsilon = \frac{m_e c^2}{2 n_e^2 k T_e}$$

The final design criterion investigated in this study is the requirement for single-pass absorption of the wave. In the cases examined so far, this is always the most restrictive criterion, since the absorption of fast waves is typically not very strong. The rationale is not so much to avoid the competition with wall absorption, (although this may be more of a problem with complex wall surfaces than it now appears to be), but to avoid randomization of the wave spectrum. Although this restriction gives the lowest theoretical efficiencies by requiring the highest parallel indices of refraction, our studies indicate that the difference is frequently surprisingly small, particularly for high beta plasmas and high frequency launchers, and that there are compensating benefits, including more effective competition with other absorption mechanisms and a narrower wave launching structure.

Following Perkins [PE82], a global average damping coefficient by electrons is estimated to be:

$$\gamma_e = \frac{\sqrt{\pi}\omega}{4} \beta_e \sqrt{\epsilon} \exp -\epsilon$$

If the alpha second harmonic resonance is inside the plasma, as it would be for aspect ratios less than five, the absorption by alphas is approximated as:

$$\gamma_{\alpha} = \pi K_{\alpha} = 4 \times 10^{-4} T_{i,10}^{3.5}$$

where $T_{i,10}$ is the average ion temperature (10 keV), and K_{α} is the one-dimensional alpha velocity distribution constant, defined by linear theory as:

$$\frac{\partial f}{\partial u} = - \frac{K_{\alpha}}{u^2}$$

where u is the normalized velocity.

Once the attenuation coefficient is calculated, the attenuation per pass () is:

$$\Delta_p = \frac{2\gamma a}{v_A}$$

where a is the minor radius (m) and v_A is the Alfvén velocity (m/s):

$$v_A = 2.2 \times 10^6 \frac{B_t}{M n_{e,20}}$$

where M is the atomic mass number of the plasma fuel (2.5 for D-T), and $n_{e,20}$ is the average electron density (10^{20} m^{-3}).

The studies reported below ‘designed’ fast wave launching systems for individual machines, operating at their pressure limits, and scanning over a range of temperatures. Four different design criteria were used, designated as A,3,M and S in the labels of the curves.

- A:** The average parallel index of refraction is selected to be 1.1 times the minimum parallel index of refraction that satisfies the accessibility requirement. Over all the plasmas we have examined, this requirement is the least restrictive.
- 3:** The average parallel index of refraction is selected to be 3 times the electron thermal velocity.
- M:** The average parallel index of refraction is selected so that the maximum current density that can be carried by a Maxwellian equals that required by the plasma.
- S:** The average parallel index of refraction is selected for single pass absorption. Over all the plasmas we have examined, this requirement is the most restrictive.

1.1.3 Theoretical Efficiency of Fast Wave Current Drive

The theoretical efficiency of the fast wave current drive is taken from two papers by Fisch and Karney. The first, “Current generation with low-frequency waves” [F181], gives a simple equation for the efficiency of transit-time pumping, which applies to the fast waves considered in this study:

$$\frac{J}{P} = \frac{13}{w_a} + 1.4 w_a + 5.$$

where w_a is the normalized parallel velocity (v_{\parallel}/v_{Te}). J/P is a normalized current density per unit current drive power that can be related to actual current and power (A/W) by the relation:

$$\frac{I}{P_d} = \frac{0.02 T_{e,10} J}{R_o n_{e,20} P}$$

The 1984 paper by Karney and Fisch [KA84], takes into account finite temperature effects, and supersedes the earlier study, except that it doesn't provide a simple equation that can duplicate its results. The method I have used to attempt to duplicate Karney's results is as follows. Equation 28 gives an analytical expression for a normalized current drive efficiency at $n_{\parallel} = 1$:

$$\frac{J}{P} = 1. + 2.5 \Theta + H_{bz} \Theta^{1.5}$$

where Θ is the electron temperature, normalized to 511 keV, the rest mass of an electron. H_{bz} is tabulated for three values of Z_{eff} . A correlation that fits this table is:

$$H_{bz} = 21.1 Z_{eff}^{-0.7}$$

The normalized J/P is equal to 1 at low temperature. Since the shape of the published curves in the 1984 Karney paper is the same as that in the 1981 paper, we assume that the correction term for a given temperature at arbitrary parallel index of refraction is the same as that at $n_{\parallel} = 1$.

1.1.4 Lower hybrid current drive model

The efficiency of lower hybrid current drive is scaled from a simplified model suggested by Rutherford for INTOR [RU82]. Rutherford assumes that 16 keV will give the highest Q, and thus fixes $T_{i,10}$ at 1.6. Similarly, Rutherford assumes an average electron tail energy of 100 keV, while discussing the constraints on lower-hybrid wave penetration and damping. We impose the penetration constraints, selecting the lower value of the index of refraction of the launched wave $n_{1\parallel}$ to be equal to the minimum value that will not convert into a fast wave before propagating into the plasma center.

$$n_{1\parallel} = \sqrt{1 + \eta^2} + \eta$$

where

$$\eta = \frac{\omega_{pe}}{\Omega_e}$$

ω_{pe} is the plasma electron frequency and Ω_e is the electron cyclotron frequency.

If the parallel index of refraction is too high, the wave will interact too strongly with electrons on the outside of the plasma, exciting surface currents, and failing to penetrate the plasma. The damping criterion is expressed by Rutherford as:

$$n_{\parallel} \leq \frac{1 + \alpha}{\sqrt{\alpha(2 + \alpha)}}$$

where $\alpha = 0.12 T_{i,10}$.

We do not impose this condition on the launched wave for three reasons. In the first place, the damping mechanism is lower hybrid current drive itself. Although saturation of electron population, an early predicted phenomenon, has not been observed where it was expected, local saturation may suppress further absorption of the wave, allowing penetration to the center. Second, the effect of unpeaked current densities may be a gradual, mild effect on achievable β , perhaps even favorable at very high beta. Third, this phenomenon simply hasn't been observed experimentally, and one can only study the reactor implications of its existence or nonexistence if it is not imposed as a constraint. Our method here is to fix the ratio of $n_{2,\parallel}$ to $n_{1,\parallel}$ at 1.2:1 and to plot $n_{1,\parallel}$, $n_{2,\parallel}$ and n_{max} for each reactor, where we are comparing reactors, and for each density, where we are looking at a single reactor, so that we can observe whether we are violating the absorption constraint and by how much.

1.1.5 Ignition and Burn Margins

For any given machine, much of the temperature range scanned may not be accessible without further auxiliary heating, because of excessive transport and radiation losses. Some insight is gained into the relative range of accessibility, by plotting ignition and burn margins, where the ignition margin is defined as:

$$MI = \frac{P_{\alpha}}{P_{t,fsl}}$$

where P_{α} is the alpha power deposited in the plasma and $P_{t,fsl}$ are the transport losses, according to various scaling laws that have been suggested. The burn margin is defined as:

$$MB = \frac{P_{\alpha} + P_{I,drive}}{P_{t,fsl}}$$

The burn margins plotted below are all for the case of fast wave current drive, using the design criterion of adequate electron population in a Maxwellian tail, and ignoring competition with alphas. The transport laws used below are neoalcat, Mirnov, Asdex-H (noncontinuous), Goldston and Perkins. A check is also made to make sure that the generally ignored neoclassical ion losses are not significant. The neoalcat electron energy confinement time (s) is given by Wolfe as:

$$\tau_{Ee,neoalc} = 0.057 n_{e20} R_o^{2.3} \sqrt{\kappa} a^{0.8}$$

The Mirnov global energy confinement time (s) is taken from last year's TFCX studies as:

$$\tau_{E,Mirnov} = 0.39 a I_p$$

The global energy confinement times predicted by Asdex-H, Goldston and Perkins scaling are taken from a recent compilation by Peng for INTOR. The Asdex-H global energy confinement time (s) is:

$$\tau_{E,Asdex-H} = 0.065 I_p R_o \sqrt{M}$$

where M is the atomic mass number of the plasma. The Goldston global energy confinement (s) is:

$$\tau_{Goldston} = 0.033 \frac{I_p \sqrt{\kappa} M R_o^{1.75}}{a^{0.37} P_\alpha}$$

where P_α is the alpha power (MW). The Perkins global energy confinement time (s) is:

$$\tau_{Perkins} = 0.13 B_t^{-0.1} P_\alpha^{-0.6} I_p^{0.9} n_{e20}^{0.6} a^{0.4} R_o^{1.7} \sqrt{M}$$

Peng's compilation also includes a simplified expression for neoclassical ion transport losses:

$$\tau_{i,neoclass} = 0.13 I_p^2 \frac{\sqrt{T_{iav}} R_o M}{n_{i,20} \sqrt{a}}$$

In all the cases reported below, this loss term is trivial over the entire range of temperatures considered, in comparison with the alpha power.

For the profiles assumed above, the thermal energy stored in the plasma (MJ) is approximately:

$$E_p = \frac{5}{4\pi} V_p \beta_t B_t^2$$

This gives transport losses (MW) of:

$$P_{t,fsl} = \frac{E_p}{\tau_{E,fsl}}$$

and ignition and burn margins as defined above.

2.0 Mission II Reactor Studies

2.1 JET

2.1.1 JET: Model

A possible set of parameters for current drive experiments on JET is shown in Table I.

Table I - JET-simulation

| Parameter | Description | Value | Units |
|-----------|----------------------------------|-------|-------|
| R_o | major radius | 2.96 | (m) |
| a | minor radius | 1.25 | (m) |
| κ | plasma elongation | 1.6 | () |
| Δ | plasma triangularity | 0.3 | () |
| B_t | toroidal field on axis | 3.45 | (T) |
| q. | engineering plasma safety factor | 4.8 | () |
| β_t | volume average toroidal beta | 4.55 | (%) |
| I_p | plasma current | 5.34 | (MA) |

The ultimate performance of JET is still to be determined. I selected a 5 MA plasma for simulation, instead of the possible ultimate performance of a 7 MA plasma, both because of the greater credibility and because it has some very desirable features as a current drive experiment. Given the limitations in heat removal and budget, the lower current has less fusion and current drive power, as well as lower cost. It also limits the beta to the 4-5 % levels at which both slow wave and fast wave experiments are possible. If the heat removal and impurity level problems were solved, JET is a surprisingly good-looking test bed for current drive. The perception from our previous studies that low aspect ratio machines gave bad steady-state current drive plasmas was based on the fact that they required high currents at low safety factor, and that the high betas prevented slow wave penetration. However, if you already have a machine that wasn't designed for low safety factor, those considerations are somewhat cancelled, making the JET plasma surprisingly similar to the Magic5 plasma described below, having twice the aspect ratio and half the safety factor.

2.1.2 JET: Results

As explained above, the principles of fast wave current drive are not entirely clear. One of the purposes of this study is to help clarify them, by exploring fast wave design using four different design criteria. As shown in Figure 1, the parallel index of refraction used for an experiment on JET varies widely depending on the reference temperature of the experiment, and whether one designs to the criteria of minimum accessibility, adequate electron population in a Maxwellian tail, three times the thermal velocity or single pass absorption. For the low frequency approach, the layer where the lower hybrid frequency equals the launch frequency is so close to the plasma edge that the accessibility limit is essentially equal to one for all cases. The assumption that three times the thermal velocity is essentially the same thing as having an adequate electron population is an excellent assumption for JET. As will be seen below, the identity between these two design criteria is less pronounced at very high beta. Single-pass absorption can be seen to be much harder to satisfy for JET than the other design criteria. Figure 2 shows the fast wave power required to drive 4.67 MA in JET, with no competition from other absorption mechanisms. The power requirements are very small. With the most stringent requirement of single-pass absorption, only 9 MW would be required at 13 keV. The simple, global model of alpha absorption suggested by Perkins [PE82] would make the situation much worse, as shown in Figure 3. Of the four design criteria, only single-pass absorption could provide all of the plasma current at less than 30 MW. Notice that the relative efficiencies of the four designs are reversed when alpha absorption is included, since the designs with lower n_{\parallel} and higher theoretical efficiencies are absorbed much less strongly than the designs with higher n_{\parallel} . The Q_{\parallel} achievable with a wave at the accessibility limit, reaches a peak of 15.1 at 18 keV, as shown in Figure 4. However, such a wave would require an extremely large anomalous enhancement of its tail population to work. At 20 keV, the Maxwellian tail population would give a Q_{\parallel} of 7.9. The simple competition with alphas gives a maximum Q_{\parallel} of 2.88, using single-pass absorption, as shown in Figure 5. Note, however, that the single-pass absorption wave was sized for single-pass absorption without competition from alphas, and would thus be absorbed in less than one pass in the presence of alphas. Although the Q_{\parallel} of 2.88 is not very good, it is better than one might have expected. Since we didn't do a scan of all possible indices of refraction, the best Q_{\parallel} achievable in the presence of alphas has to be somewhat higher. One of the questions that need to be answered by more sophisticated techniques is where to place the alphas in a global approximation. If the aspect ratio is five or greater, the alpha second harmonic, which equals the deuterium second harmonic, is entirely outside of the plasma, and thus should not act strongly with the fast wave. However, if the aspect ratio is less than five, but close to five, the alpha second harmonic layer may

be sufficiently close to the edge that the alpha population is greatly depleted, so that competition with alphas might be considerably less than that envisioned in a global approximation. JET has an aspect ratio of 2.37 in this experiment, so alpha depletion toward the edge is probably irrelevant. The other tokamak plasmas considered here have aspect ratios of 3.5 (TIBER), and 3.7 (ET-II), where the effect might be more helpful. The Magic5 reactor has an aspect ratio of five, in order to avoid competition with alpha and ion harmonics altogether. The currents/watt implied by these power requirements are shown in Figure 6. All four design methods can provide theoretical efficiencies of better than 1 A/W at reasonable (< 20 keV) temperatures. The theoretical efficiency of the Maxwellian tail vs. temperature is shown in Figure 7, according to the cold plasma theory of Fisch and Karney [FI81] and the hot plasma correction of Karney and Fisch [KA84]. As can be seen, the difference between the two only becomes significant at high temperatures (> 20 keV). Without the favorable correction term, however, the normalized $\langle J/P \rangle$ would be no higher than 27 at any temperature, and only reaches 31.4 at the high temperature. The hope that fast wave current drive might reach $\langle J/P \rangle > 40$ is made difficult by adding the requirements of Maxwellian tails or single pass absorption. However, after examining the four tokamaks discussed here, as well as looking at the implications of previous trade studies with the slow wave [SC84], it becomes clear that the real advantage of the fast wave over the slow wave is not the higher $\langle J/P \rangle$ at low index of refraction, but its ability to penetrate high beta plasmas. Above a beta of 5 %, it appears that the slow wave will not penetrate to the center of a tokamak plasma. Figures 8,9, 10 are included primarily for reference, showing peak fusion powers for JET for the experiment described of 44.1 MW, a peak neutron wall loading of 0.2 MW/m², and an average electron density at an average electron temperature of 6 keV (peak = 13.2 keV) of 1.05×10^{20} m⁻³, or about three times the Murikami limit in the ohmic regime. It should be noted that these values are based on the self-consistent scaling laws, used for parametric sizing studies by the author [SC84], and are not based on a careful consideration of JET performance to date. Figure 11 shows ignition margins, according to various scaling laws. The top of the curve is an ignition margin of one, indicating that these laws don't predict that JET ignites at 4.67 MA. Mirnov scaling does the best, with a peak of 0.82. In a driven experiment, however, thermal equilibrium only requires a burn margin greater than one. For a fast wave, driven by Maxwellian electrons, a burn margin greater than one is satisfied over a broad temperature range by Mirnov scaling at lower temperatures (and higher current drive powers) for neoalcalator, Asdex H-mode, and Goldston scalings, but not for Perkins, as shown in Figure 12. Purchasing 15-20 MW of current drive equipment, however, would allow a broad range of temperatures under a wide variety of scalings. The number of passes needed for

absorption, without competition from alphas, varies very strongly with the selection of the index of refraction, as shown in Figure 13. Even with 100 steps in n_{\parallel} at every temperature in our code, there is strong "ratcheting" in the results. Notice that the subtle difference between three times thermal and a Maxwellian population can make a first-order difference in the predicted number of passes for absorption. The number of passes for the minimum accessibility wave for all four machines is even higher than the typical vacuum cavity Q's of a few hundred, and appears to be a very good reason not to use the minimum accessibility criterion for design. Even the Maxwellian and 3 times thermal criteria are highly questionable as to whether they would retain any "memory" of their initial phase velocity after so many passes.

The basic launching structure for current could be considered to be the four-element waveguide grid. Antennas may be used, but are not known to be compatible with high neutron fluxes. Other, cleverer launching structures, such as waveguides with complex shapes have been proposed, in order to take up less space. However, the the width of a 4 element waveguide array is still interesting, as being the most straightforward design solution, when feasible. For the JET plasma, only the single-pass absorption option would give an array with a width less than one meter, as shown in Figure 14. This, then, can be another important advantage of the high parallel index of refraction design, along with its stronger absorption.

The efficiency of slow-wave current drive is evaluated, using the same techniques described for the sizing studies [SC85], holding $n_{\parallel,1}$ to exactly the value that would give mode conversion at the center, and setting $n_{\parallel,2}$ to $1.2 n_{\parallel, n_{max}}$ for penetration of the wave to the center in competition with damping by electrons is merely displayed, not used as a design criterion. The Q according to the global expression $Q=0.88 \kappa B_t a$, suggested by Rutherford [RU82] is shown for purposes of reference, not because it was meant to be true at every temperature, but because it represents the implications of previously made simplifying assumptions, and thus provides a point of reference when we find behaviour either better or worse than might have been expected. If n_{max} is not higher than $n_{\parallel,2}$ some of the wave will be damped toward the edge. If it is not higher than $n_{\parallel,1}$, all of the wave will be edge damped. Using this design criterion, a Q of 8.2 could be achieved with slow wave current drive at a temperature of 19 keV, as shown in Figure 15. Only about 4 MW of current drive should be required! However, at this temperature, every scaling law predicts that auxiliary power would be needed to supplement alpha and current drive power. As can be seen in Figure 16, the JET plasma described here, having a beta less than 5 %, allows good penetration of the slow wave, out to temperatures above 20 keV. It can now be seen why we limited ourselves to only 4.67 MA, when JET may some day achieve 7 MA or higher. At the lower current and

beta, both fast wave and slow wave experiments are possible, and it is more likely that the thermal problems associated with steady-state current drive might be solvable. If they are, there is nothing in this simulation that indicates that JET would not be a very good target plasma for steady-state current drive.

2.1.3 JET: Conclusions

- Slow-wave penetration of a 4.6 % beta plasma would be fairly deep, out to temperatures approaching 20 keV. At 16 keV, a Q of 7.6 is predicted, corresponding to only 6-7 MW of lower hybrid power! (Note that 24 MW is required at 8.5 keV, where the plasma has the maximum fusion power, for the assumed profiles. An improvement of a factor of two can be explained by the halving of the density. The other factor decreasing the power requirement is that the n_{\parallel} required for a Maxwellian decreases from 2.5 to 1.6.) Auxiliary power would be required to give a burn margin of one.
- A theoretical Q of 6 at 16 keV is also achievable with fast wave current drive, with no alpha competition, with a Maxwellian electron population. With competition from alphas, the maximum achievable Q is worse than that for TIBER (since JET is the lowest aspect ratio machine considered in this study, the alpha second harmonic layer would also be closest to the center for fast current drive at $2.5 \omega_{c,D}$), limited to Q = 3 for single-pass absorption.
- If the engineering and political difficulties of designing a slow wave/fast wave experiment for JET can be solved, it may be an adequate test bed for a definitive experiment, and would almost certainly be a very good target plasma for a pre-TFCX or Mission II set of experiments. The frequency of the low frequency wave at $2.5 \omega_{c,D}$ would equal 65.7 MHz at 3.45, which has the added benefit of being within the tuneable range of the JET ICRF heating system.

2.2 TIBER

2.2.1 TIBER: Model

A simulation of a TIBER-like tokamak was done, using the global parameters shown in Table II. The dimensions are identical with those of TIBER, but the calculated values of beta and plasma current are slightly less, by around 15 %.

Table II - TIBER-simulation

| Parameter | Description | Value | Units |
|-----------|----------------------------------|-------|-------|
| R_o | major radius | 2.73 | (m) |
| a | minor radius | 0.745 | (m) |
| κ | plasma elongation | 1.6 | () |
| Δ | plasma triangularity | 0.43 | () |
| B_t | toroidal field on axis | 5.0 | (T) |
| q | engineering plasma safety factor | 2.2 | () |
| β_t | volume average toroidal beta | 10.36 | (%) |
| I_p | plasma current | 10.0 | (MA) |

2.2.2 TIBER: Results

The curves of index of refraction vs. temperature are similar for all four tokamaks in that they all go down with temperature, three times thermal appears to be close to a Maxwellian tail population and the accessibility limit is close to one. However, for TIBER, there is a puzzling dip in the single-pass absorption curve at low temperatures that does not appear for the other tokamaks, as shown in Figure 17. We suspect that this is caused by a bug in the numerical model and has no physical basis, but have not discovered the cause. Except in the glitch area, the value of $n_{||}$ for the four criteria appears to be about the same as for JET at all temperatures. The next three machines are Mission II devices. Each generates considerably more fusion power than JET at low beta and thus the corresponding current drive power is also higher. As seen in Figure 18, a restriction of 30 MW for a fast-wave experiment on TIBER, even without any competitive absorption mechanisms, would require a temperature of about 20 keV for a Maxwellian tail or for single-pass absorption. This is not inconsistent with Logan's proposal to do fast wave current drive at 20 keV. The power requirements with global competition with alpha absorption is much worse, as shown in Figure 19, with single-pass absorption again being the best of the four design options. A theoretical Q of 17.6 could be reached with a wave at the accessibility limit, as shown in Figure 20. At 20 keV, a plasma with a Maxwellian tail would have a Q of 9.3, implying that it might not be necessary to raise the temperature as high as 30 keV, as proposed by Logan, in order to achieve a Q > demonstration experiment on TIBER. With global competition from alphas, single-pass absorption gives a maximum Q of 4.24 at a temperature of 15 keV, at an absorbed current drive power level of 60 MW, as shown in Figure 21. While 60 MW is not good enough, it is again surprising how well

the single-pass absorption option did, suggesting further scanning of the range of higher indices of refraction. The theoretical efficiency, expressed in terms of amperes/watt, shown in Figure 22, is 3-4 times worse than that of JET. Since the two machines have nearly identical major radii, the difference comes from the fact that TIBER has a much higher density, due to its higher beta and field. As seen in Figure 23, the difference does not come from any differences in J/P, which are essentially identical for the two machines. The maximum fusion power for TIBER is shown in this simulation to be 331 MW, and the maximum neutron wall loading 2.1 MW/m^2 , as shown in Figures 25 and 26. These values are close to those calculated by Livermore. The density, however, at 6 keV is $4.32 \times 10^{20} \text{ m}^{-3}$, four times that of JET, as shown in Figure 26. The multiplier over the Murikami limit, however, is only slightly higher than that in JET, because of the lower major radius and safety factor and the higher field in TIBER. The calculation of ignition margins vs. temperature appears to be slightly more optimistic than that of Livermore. Ignition margins of greater than 1.5 are shown, for Mirnov, neoalculator, and Asdex H-mode, but not for Goldston and Perkins, as shown in Figure 27. An ignition margin greater than one is shown out to 26 keV for Mirnov and Asdex-H mode. For TIBER, Asdex H-mode and Mirnov scaling are indistinguishable. Neoalculator scaling shows an ignition margin higher than one out to 21 keV. Burn margins greater than one extend past 31 keV and even exceed Goldston scaling out to 12 keV, as shown in Figure 28. These results are compatible with Logan's calculation of a subignited, stable burn at 30 keV.

The number of passes needed to absorb a Maxwellian are about half the number required for JET, with 20 passes needed to absorb a wave at three times the thermal velocity at 20 keV, as shown in Figure 29. The width of a four element array is somewhat less than that for JET, because of the higher field, as shown in Figure 30, allowing a low frequency wave with a frequency as high as 95 MHz. Under 75 cm would be needed for a four element array designed for single pass absorption at any temperature under 31 keV.

The maximum Q for the slow wave, limited to mode conversion at the center, is 6.9, as shown by Figure 31. However, because of the high beta of TIBER, the slow wave would be damped entirely on the edge, as shown in Figure 32. As stated before, the "edginess" of a thermonuclear plasma is almost entirely a function of beta only. Since TIBER has a higher beta than STARFIRE, it's slow wave current drive would be even more towards the edge than STARFIRE's if such a thing is possible. Thus, the TIBER plasma has little chance of being a good slow wave current drive demonstration.

2.2.3 TIBER: Conclusions

- For a plasma, such as TIBER, with beta in the 10 % range, the slow wave would be absorbed

entirely on the plasma edge. A wave meeting the requirement of avoiding mode conversion before the plasma center would have a theoretical Q of 6.6 at 21 keV.

- A theoretical maximum Q of 17.5 is predicted at the accessibility limit at 18 keV, using low frequency, fast-wave current drive. However, this wave competes poorly with other absorption mechanisms and doesn't satisfy the criterion of having an adequate Maxwellian tail population. If the criterion of adequate tail population were satisfied, the Q at this temperature would be exactly half that, or 8.8. The fusion power would be 62 % of the maximum power, and the burn margin would be greater than one for Mirnov, neoAlcator, and Asdex-H scalings, but not for Goldston and Perkins. This is perhaps the most attractive-looking experiment for this machine, subjectively trading-off desirability vs. credibility, being close in performance to the $Q=10$ experiment, being suggested by Livermore. The slightly higher $n_{||}$ guarantees an adequate electron population, and the slightly higher power increases the probability that the burn margin will be greater than 1.

- The best performance with linear, global competition vs. alpha absorption is achieved with the highest $n_{||}$ considered, which is that needed for single-pass absorption. This performance, however, is inadequate, peaking at $Q=4.4$. A more sophisticated treatment of alpha absorption is clearly required before going further, since this level of performance would make the experiment a failure. It would also be interesting to optimize Q vs. $n_{||}$ for competition with alpha absorption, since this has not yet been done.

- TIBER's ignition margin is perhaps less marginal than has been indicated by the point design. TIBER satisfies Mirnov, ASDEX-H and neoAlcator scaling over a broad range of temperatures. Backing off on temperature a little gives a significant improvement in ignition margin, for a given fast wave experiment; while only causing a second-order decrease in the efficiency of the current drive.

- However, TIBER fails to persuade that it is a well-designed, fast-wave ignited burn experiment. It could be improved upon in three ways:

- (1) It cannot easily compete with alpha-absorption. A higher aspect ratio ($A=5$) machine could avoid competition with the alpha second cyclotron harmonic, altogether.
- (2) The important psychological goal of achieving $Q=10$, identified by Livermore, could be thwarted by an inadequate electron tail population.
- (3) It has too high a beta to allow a credible backup or supplement (to avoid thermal instabilities or to broaden profiles) from the slow wave. It is thus, on three counts, a very high-risk experiment. All three of these shortcomings are eliminated by the Magic5 plasma, described below.

2.3 Magic5

2.3.1 Magic5: Model

An aspect ratio of 5 has a certain magic about it for a steady-state mission II device for the following reasons:

- At $A=5$, low frequency fast wave experiments can be done without any interference from alpha or fusion fuel cyclotron harmonics. At $A=5$, and an elongation of 1.6, beta is limited to about 4 %, at which level lower hybrid slow waves can still penetrate the fusion plasma. At a beta of 5 %, penetration is already becoming restricted at thermonuclear reactor temperatures.
- At $A=5$, previous costing studies show no first order cost penalty vis-a-vis the cost optimum, without even considering costs associated with current drive. In a recent study, using the Fusion Engineering Design Center tokamak system code [RE85], holding ignition margin constant, an $A=5$ machine cost 16 % more than an optimum aspect ratio machine, neglecting current drive. (The system code also neglects several other current-related cost factors, such as the design against disruption of the vacuum vessel, armor, limiters, collectors, launching structures and superconducting magnets. We, therefore, suspect an untrue bias towards lower aspect ratio machines.) However, $A=5$ probably is higher than the optimum cost aspect ratio, so there is little motive for increasing the aspect ratio any further.
- It is sometimes claimed that the collaborative process of establishing consensus on next-step tokamaks has led repetitively to the selection of middle of the aspect-ratio solutions in the past. Clearly the only alternatives are high and low aspect ratios. A previous study established that there are no attractive solutions for super-low aspect ratio alternatives for Mission II, because of the maximum field limitations on superconducting magnets, and the fundamentally poor field utilization of super-low aspect ratio machines. Since an aspect ratio of 4.9 is still a medium aspect ratio machine in the eye of all observers, $A=5$ is the smallest high aspect ratio machine one can build.

An attractive-looking $A=5$ device was selected from the tabulation of 206 possible Mission II tokamaks in a separate report by the author [SC85]. The machine described below has a major radius less than 4.0 m. and a plasma current of less than 6.0 MA. It has an ignition margin greater than 1.5 for Mirnov, neoAlcator and Asdex-H scaling, but an ignition margin less than 1.0 for Goldston and Perkins scalings. The maximum field on the TF magnets is 10.8 T. This reactor is similar in size to the nominal performance TFCX-S option, studied in FY85, but it has the additional mission of steady-state current drive. Despite the second mission, the FEDC tokamak systems code predicts a total cost that is \$50 M less than that of TFCX-S.

Table III - Mission II, A=5 Steady-state tokamak simulation

| Parameter | Description | Value | Units |
|-----------|----------------------------------|-------|-------|
| R_o | major radius | 3.95 | (m) |
| a | minor radius | 0.79 | (m) |
| κ | plasma elongation | 1.6 | () |
| Δ | plasma triangularity | 0.3 | () |
| B_t | toroidal field on axis | 6.88 | (T) |
| q. | engineering plasma safety factor | 2.1 | () |
| β_t | volume average toroidal beta | 4.05 | (%) |
| I_p | plasma current | 5.98 | (MA) |

2.3.2 Magic5: Results

The parallel indices of refraction for Magic5, shown in Figure 33, are similar to those for TIBER and JET. The power requirements for Magic5, shown in Figure 34, are somewhat lower than those for TIBER for each design option, reflecting the slightly higher Q. The power requirements in competition with alpha absorption are also somewhat lower, but still unacceptable, as shown in Figure 35. The maximum Q of fast wave satisfying the accessibility requirement is 19 at 18 keV, which is 1.5 higher than TIBER and 4 higher than JET. A Maxwellian at 20 keV has a Q of 10.1, and thus would achieve the goal of a Q=10 experiment, that is slightly missed by TIBER. (Of course, the fundamental uncertainties in calculating the absolute value of Q are much larger than the differences between Magic5 and TIBER. However, since getting from Q=10 to Q=20 involves an uphill, percentage by point struggle, predicted fractional differences may be of some significance.) The Q with global competition with alphas of 3.5 is worse than that of TIBER, as shown in Figure 37. However, with the low frequency option specified, there is no competition with alphas in Magic5, because the alpha cyclotron resonance is outside the plasma. The efficiency of current drive of Magic5 with a Maxwellian tail, expressed in amperes/watt is slightly worse than TIBER, because of the higher major radius, as shown in Figure 38. However, Magic5 has only 54 % as much current as TIBER, so the power levels required at any temperature are less. The $\langle J/P \rangle$ of Magic5 is negligibly better than that of TIBER. The fusion power is about the same as that of TIBER, as shown in Figure 40, while the wall loading of 1.58 MW/m² is 3/4 that of TIBER, as shown in Figure 41. The densities are slightly lower than those in TIBER, with about the same ratio to the Murikami limit as those in JET, as shown in Figure 42.

Magic5 achieves ignition margins greater than 1.5 for neoalculator, Mirnov and Asdex H-mode scaling, but does not ignite for Goldston or Perkins scaling, as shown in Figure 43. Neoalculator scaling would allow ignition out to 26 keV, while Mirnov would allow it out to 20 keV. As with TIBER, a Burn Margin greater than one would be achieved for Goldston, but not Perkins scaling, out to 11 keV, as shown in Figure 44.

The number of passes for absorption of a Maxwellian tail wave is more like JET, about double the number for TIBER, as shown in Figure 45.

The width of a four element array is comparatively small, because of the high field of Magic5, as shown in Figure 46. Even a Maxwellian would require a port only a little more than a meter wide at 20 keV, while a single pass absorption wave would only require 44 cm, opening the possibility for having even more elements in parallel for better spectrum control. The frequency equal to 2.5 times the central deuterium cyclotron frequency is 131 MHz, in the VHF range.

The slow wave lower hybrid wave would have a maximum Q of 10.7 at 18 keV. Thus, of the tokamak plasmas we have found so far, the Magic5 has the unique feature of being a possible Q=10 demonstration for either slow wave or fast wave. This also presents the possibility of making an orderly transition from a slow wave to a fast wave plasma or of mixing slow wave with fast wave current drive for a single plasma. (Perhaps the ideal way of running a steady-state tokamak is with slow-wave for the edge and fast-wave for the center.) Because of the low beta, the penetration of the slow wave is as good as that for JET, as shown in Figure 48.

2.3.3 Magic5: Conclusions

- If fast wave current drive were to be limited to less than 30 MW, the experiments would have to be performed at a temperature above 17 keV in D-D. At 20 keV, the Q of fast wave current drive, with $n_{||}$ selected to satisfy the Maxwellian electron tail population criterion is 11, or about 20 % higher than that of TIBER. This is somewhat surprising, since the beta is only half that of TIBER. The beta advantage is probably cancelled by the fact that Magic5 has 40 % higher field than TIBER.
- If there were competition with alphas, the Q would be limited to 3.65 for single-pass absorption, but at an aspect ratio of 5 and $\omega = 2.5 \omega_{c,D}$, there should be no competition.
- The predicted slow-wave efficiency of the Magic5 is that Q = 10 can be achieved at 19 keV with about half the launched spectrum accessible to the plasma center. At this temperature, the ignition margin is still higher than one for neoalculator, Mirnov and Asdex-H scaling. The lower hybrid power is approximately 20-25 MW, similar to the required fast-wave power.
- Magic5 is about the same size as last year's TFCX-S. Its TF magnet is about double the stored

energy of those of JET and TFTR. It is capable of doing the same long burn ignition experiment as last year's machines. It is also capable of attempting $Q = 10$, steady-state burn demonstrations with both fast-wave and slow-wave current drive.

2.4 ET-II

2.4.1 ET-II: Model

Of the various methods for increasing beta in the first critical beta regime, defined by the Troyon parameter, there is a fundamental difference between elongation on the one hand, and triangularity and inverse aspect ratio on the other. All three are capable of increasing beta, but triangularity and inverse aspect ratio are incapable of increasing beta, without increasing plasma current, nearly linearly, with beta. An analytical proof in a separate memorandum by the author showed that, if elongation and safety factor are increased simultaneously, beta can be increased, while current is decreased. The Mission II ET described below is a worked example, achieving a beta of 36 % with a current of only 10.2 MA. The ignition margin is greater than 1.5 for Mirnov, Asdex-H and neoAlcator scaling, but not for Perkins or Goldston scaling. The fusion power is 363 MWt, slightly higher than moderately elongated machines with ignition margins higher than 1.5 for three ignition criteria. (For $\kappa = 1.6$, a fusion power of about 300 MWt is required.) The decision made by General Atomic to pursue ET as an ohmic ignition device with a low safety factor has, so far, obscured this fundamental distinction.

Table IV - Mission II ET tokamak simulation

| Parameter | Description | Value | Units |
|-----------|----------------------------------|-------|-------|
| R_m | major radius | 2.2 | (m) |
| a | minor radius | 0.5 | (m) |
| κ | plasma elongation | 10.0 | () |
| B_t | toroidal field on axis | 2.1 | (T) |
| q | engineering plasma safety factor | 7.0 | () |
| β_t | volume average toroidal beta | 35.9 | (%) |
| I_p | plasma current | 10.2 | (MA) |

2.4.2 ET-II: Results

ET-II, because of its very high beta, differs more from the three previous tokamaks than they do from each other. The first subtle difference one notices in Figure 49, showing the parallel indices of refraction, is that the requirement of a Maxwellian electron tail and three times the thermal

velocity diverge more than in the other cases, while the requirement of single pass absorption is much more easily fulfilled. The power requirements are about a third higher than for Magic5 or TIBER, because of the higher fusion power required in ET-II to meet ignition requirements, as shown in Figures 50 and 51. The second part of the motivation for ET-II, along with its high beta, is shown in Figure 52. The theoretical Q of fast wave current drive at the accessibility limit is 27.4 at 18 keV, or 50 % higher than that of TIBER. This holds out the promise of restoring the STARFIRE goal of $Q > 30$ for commercial-size plasmas, in order to get rf power under 100 MW. The Q for a Maxwellian tail at 20 keV is 15, also 50 % better than TIBER or Magic5. The maximum Q , in competition with alpha absorption is 7, as shown in Figure 53. Notice, however, that since single pass absorption is easier (i.e. at lower indices of refraction) for ET-II than the other tokamaks, it is quite likely that significantly better performance might be obtainable at higher indices of refraction, again suggesting the need to scan this parameter more completely. The amperes/watt are somewhat higher than those for TIBER, as shown in Figure 54. $\langle J/P \rangle$ is only higher by one than that for Magic5, indicating again that it is primarily a function of temperature and a very weak function of everything else, as shown in Figure 55. The fusion power is 782 MW, as shown in Figure 56. This is the main disadvantage of the ET concept. Because some scaling laws don't favor elongation, the low minor radius makes it difficult to satisfy a variety of global scaling laws at 300 MW, the way the more conventionally shaped tokamak plasmas can. The wall loadings and densities are about the same as those of Magic5 and TIBER, as shown in Figures 57 and 58. However, the ET has a possible problem, similar to that of plasmas in the second-stability regime, which is that the densities achievable are nowhere close to those achievable in the ohmic regime. While there is no well-defined relation between the ohmic density limit and auxiliary heated and fusion power driven plasmas, a discrepancy of this magnitude (a factor of thirty) could lead to severe operational problems in getting to steady-state ignition or leaving ignition without disruption.

The ET-II satisfies Mirnov and Asdex H-mode ignition margins all the way to a temperature of 30 keV, while neocator with a $\sqrt{\kappa}$ dependence is satisfied until 21 keV, as shown in Figure 59. Goldston and Perkins scalings are not satisfied. Because of the higher Q 's, there is less of a difference between ignition margin and burn margin, but the same phenomenon that was observed before, that Goldston was satisfied out to about 12 keV is also observed for ET-II, as shown in Figure 60.

The number of passes needed for absorption of a Maxwellian is greatly reduced for ET-II to under 15, as shown in Figure 61. The separation between a Maxwellian and three times the

thermal velocity is also much greater, indicating that three times the thermal velocity shouldn't be universally used as an indicator of electron population.

Because of the very low field of ET-II, the width of a 4 element waveguide array is very large, as shown in Figure 62. With the combination of small size, low frequency (40 MHz), and small index of refraction for single pass absorption, waveguide launch appears to be totally impractical.

Even if a slow wave could get past the edge, which it certainly can't (see Figure 64), the Q of slow waves limited by mode conversion at the center would still be low, no higher than 3.2 at 20 keV. Slow waves are evidently impractical for such high beta devices.

2.4.3 ET-II: Conclusions

- The lower hybrid slow wave will not penetrate this plasma at all. Even without accessibility constraints, mode conversion would limit slow wave Q to a maximum of 3.3.
- Fast wave current drive efficiency appears to improve monotonically, although very slowly with beta. A Q of 11 is predicted at 18 keV for a wave with a Maxwellian electron tail population capable of carrying the current. This is about the same as for the Magic5 option. The maximum Q at the accessibility limit is increased from 19 to 22.
- The highest Q with averaged global competition with alphas is 6.0, which is inadequate, although the highest we have observed so far for next-step reactors. (Although not shown here, a commercial-reactor scale ET can have a predicted Q of 50 without alpha competition and 20 with. This is, perhaps, the fundamental motivation for pursuing the ET geometry further.)
- The physics of the ET-II device, described here, is significantly more speculative than that of the Magic5, without promising higher ignition margin or Q for current drive. However, the reactor relevance of a possible machine with $\beta = 36\%$, a steady-state Q greater than 10 and a major radius less than 3.0 m is obvious.

3.0 Global Conclusions

- The surprise winner in the survey of fast wave design techniques was single pass absorption which frequently showed smaller than expected disadvantages in theoretical efficiency, while exhibiting far and away the best ability to compete with the mechanisms fighting the electron tails for absorption. The smaller size of waveguides with the higher index of refraction is an additional benefit.
- It is possible to design a tokamak the size of TFCX-S that could demonstrate $Q=10$, using either the fast wave or the slow wave. The possible benefits of this extend far beyond political demonstrations.

(1) Since we don't know for sure which form of current drive is better, this gives us an opportunity to find out in one machine.

- (2) If the fast wave is better, but can't reach the steady-state operating conditions by itself, the slow wave gives it a way to get there.
 - (3) Fast waves are better at heating the center and high beta plasmas, while slow waves are better at heating the edge and low beta plasmas. We don't really know the current and temperature distributions we want in the optimum plasma. Having both waves available gives us the control we need to optimize Q and beta.
 - (4) The fast wave may very well have a higher Q, but be grossly unstable, because of its strong positive beta dependence. It may be necessary to supplement the fast wave by the slow wave whose penetration has a negative beta dependence in order to have stable current drive
- All of this points to the possibility of doing fast wave and slow wave current drive on the same tokamak, and perhaps even with the same rf equipment, i.e. at the same frequency. Competition with alphas would now be necessary again. This may or may not be the correct reactor concept, but would be a definitive physics experiment for high frequency current drive. We believe this could be easily implemented with square waveguide, horns and twistguide transition sections.

References

- [F184] N.J. Fisch and C.F.F. Karney. "Current generation with low-frequency waves", Phys Fluids 24(1), 1981
- [KA84] C.F.F. Karney and N.J. Fisch. "Efficiency of current drive by fast waves", Princeton Plasma Physics Laboratory Report PPPL-2128, 1984
- [PE82] F.W. Perkins, "Fast Wave Current Drive: Prospects for a Purely Steady-State FED", published in some INTOR document
- [SC85] R.L. Reid et al, "The Tokamak Systems Code", Fusion Engineering Design Center Report, ORNL/FEDC-84/9, March 1985
- [RU82] P.H. Rutherford et al, "Application of Lower-Hybrid Current Drive to an FED/INTOR-Like Device," 1982, unpublished
- [SC85] J.H. Schultz, "Parametric Studies of Next-Step Superconducting Tokamak Experiments at Constant Wall-Loading", MIT Plasma Fusion Center Report, PFC/RR-81-1, Jan 1985

$R_0=2.96$ m, $a=1.25$ m, $B_t=3.45$ T, $\kappa=1.6$
 $q_{lim}=4.8$, $I_p=4.67$ MA, $\beta_{av}=4.0$ %

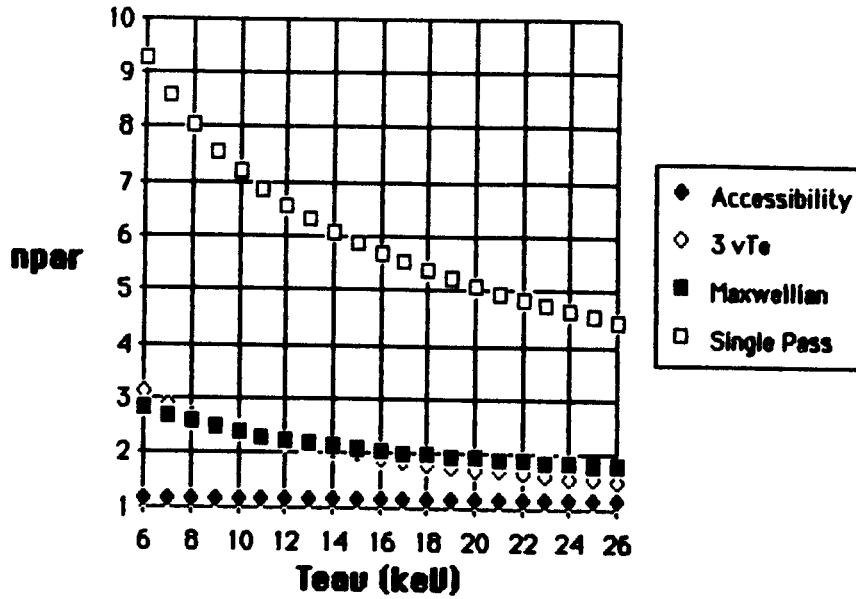


Figure 1
Parallel Indices of Refraction vs. Average Temperature (keV)

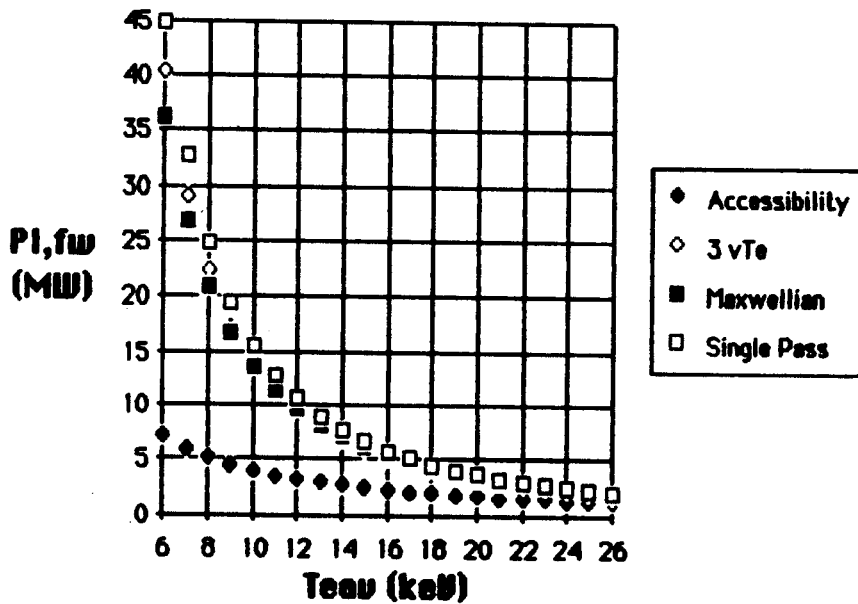


Figure 2
Required Fast Wave Power, no alphas (MW) vs. Temperature (keV)

$R_0 - 2.96 \text{ m}$, $a - 1.25 \text{ m}$, $B_t - 3.45 \text{ T}$, $\kappa - 1.6$
 $q_{lim} - 4.8$, $I_p - 4.67 \text{ MA}$, $\beta_{av} - 4.0 \%$

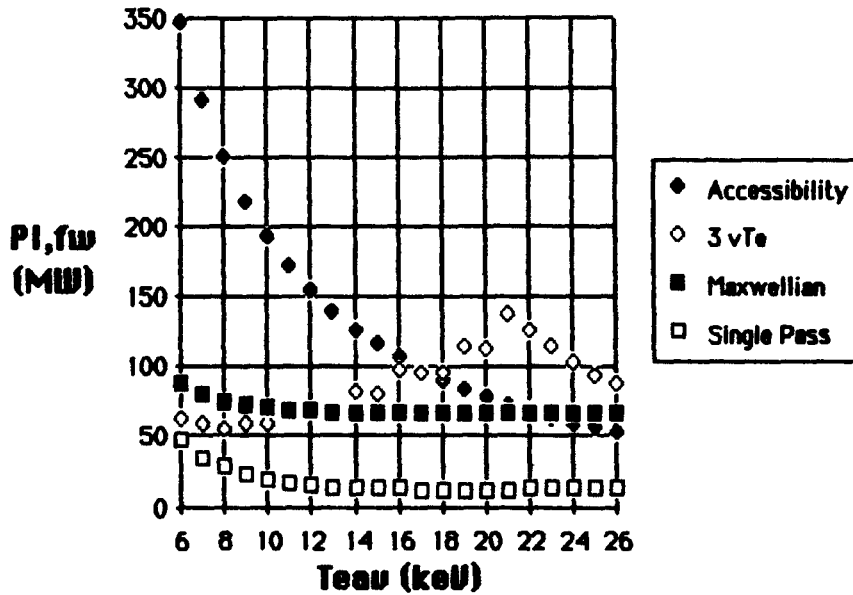


Figure 3
Required Fast Wave Power, with alphas (MW) vs. Temperature (keV)

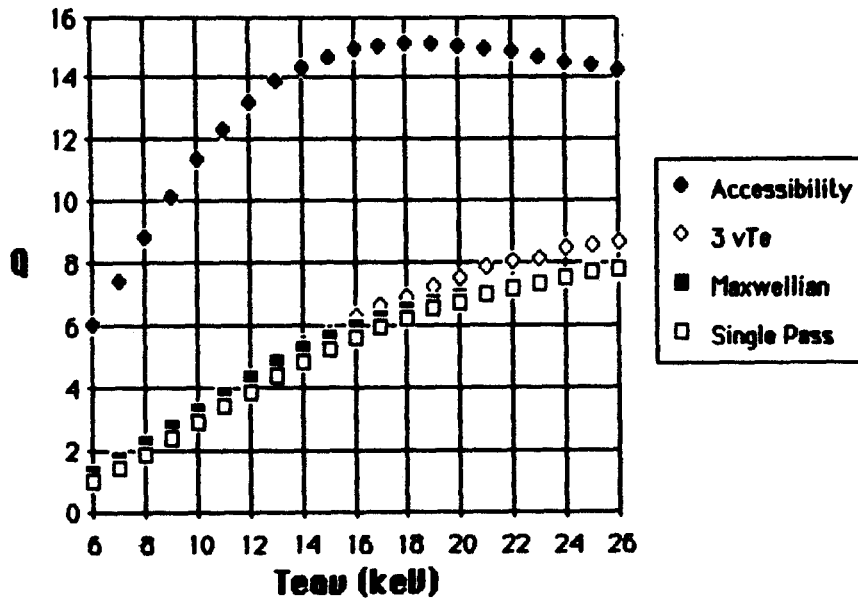


Figure 4
Q of Fast Wave Current Drive, no alphas vs. Average Temperature (keV)

$R_0 = 2.96$ m, $a = 1.25$ m, $B_t = 3.45$ T, $\kappa = 1.6$
 $q_{lim} = 4.8$, $I_p = 4.67$ MA, $\beta_{av} = 4.0$ %

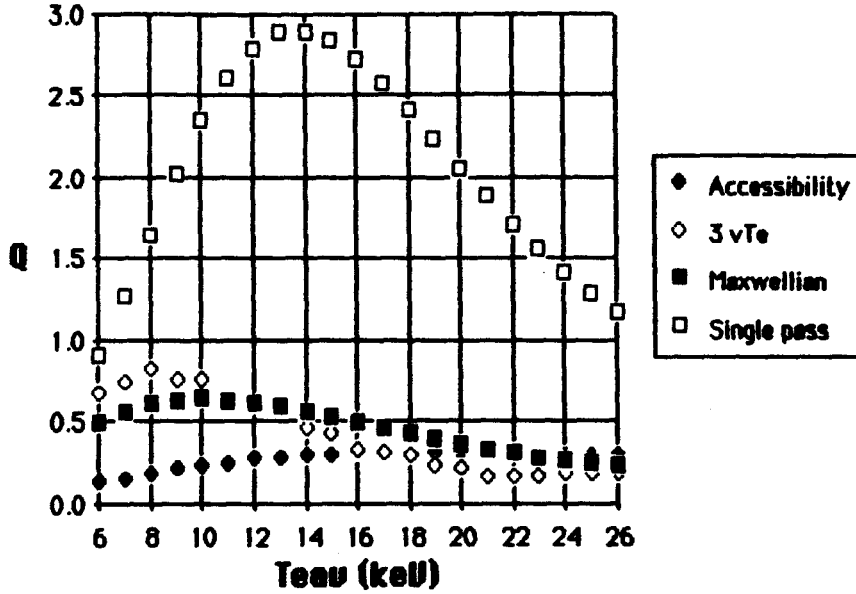


Figure 5
Q of Fast Wave Current Drive, with alphas vs. Temperature (keV)

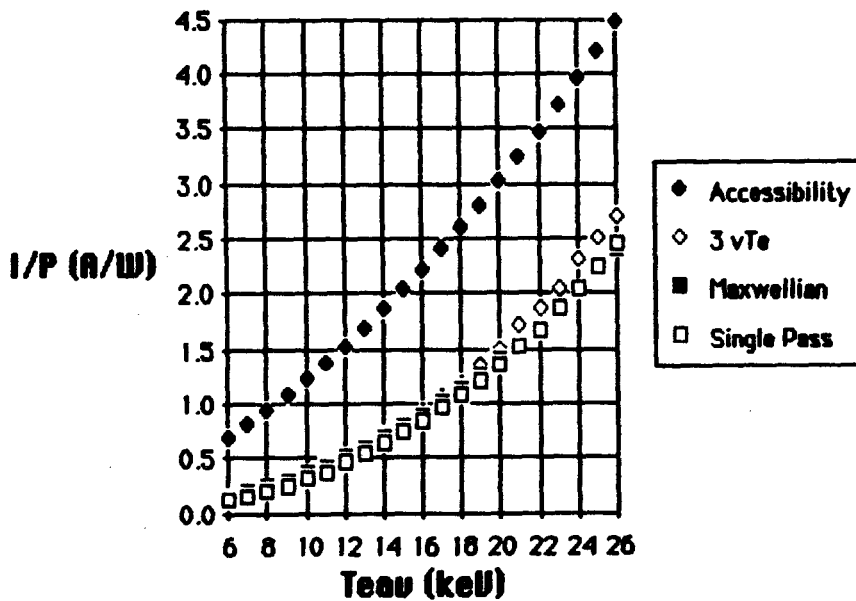


Figure 6
Fast Wave I/P, no alphas vs. Average Temperature (keV)

R_0 -2.96 m, a -1.25 m, B_t -3.45 T, κ -1.6
 q_{lim} -4.8, I_p -4.67 MA, β_{av} -4.0 %

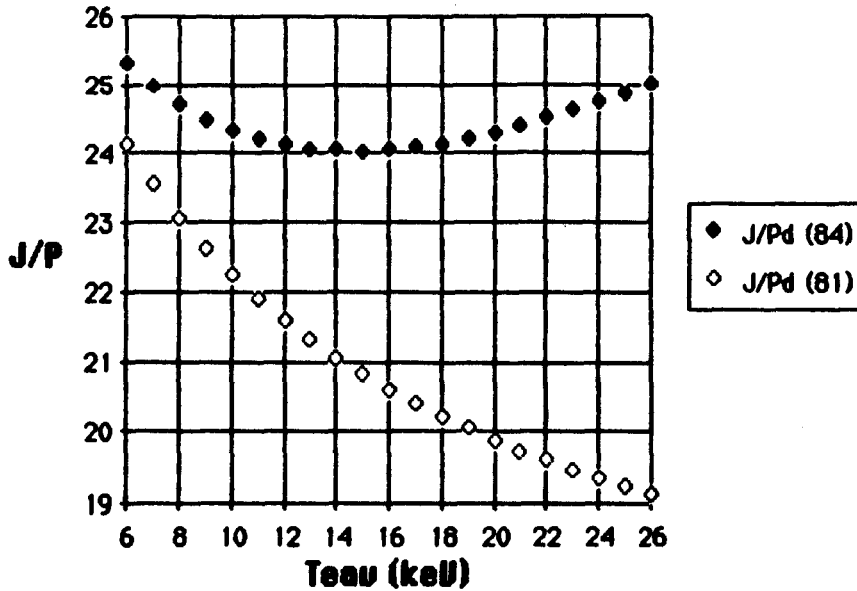


Figure 7
Normalized J/P (Karney/Fisch, 1984, Fisch/Karney, 1981)
Maxwellian Tail, no alphas
vs. Average Electron Temperature (keV)

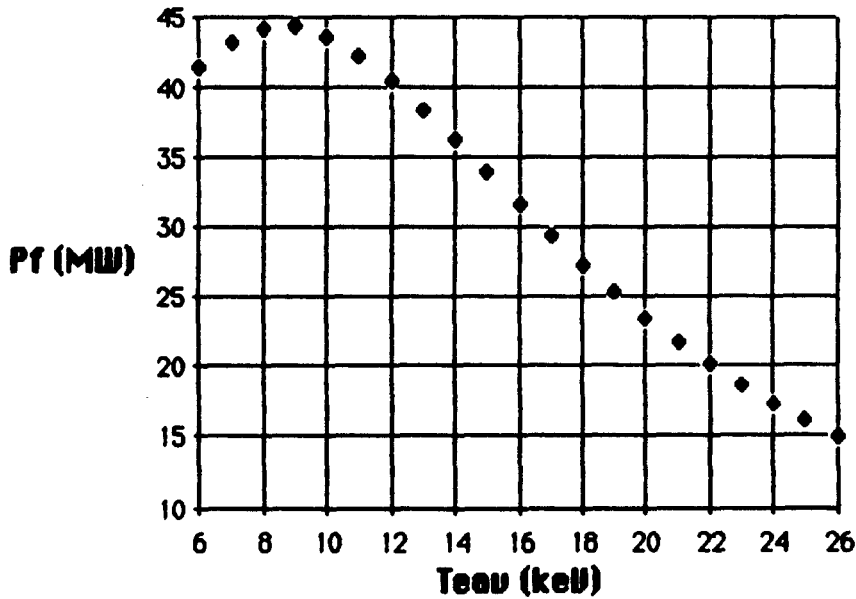


Figure 8
Fusion Power (MW) vs. Average Electron Temperature (keV)

R_o -2.96 m, a -1.25 m, B_t -3.45 T, κ -1.6
 q_{lim} -4.8, I_p -4.67 MA, β_{av} -4.0 %

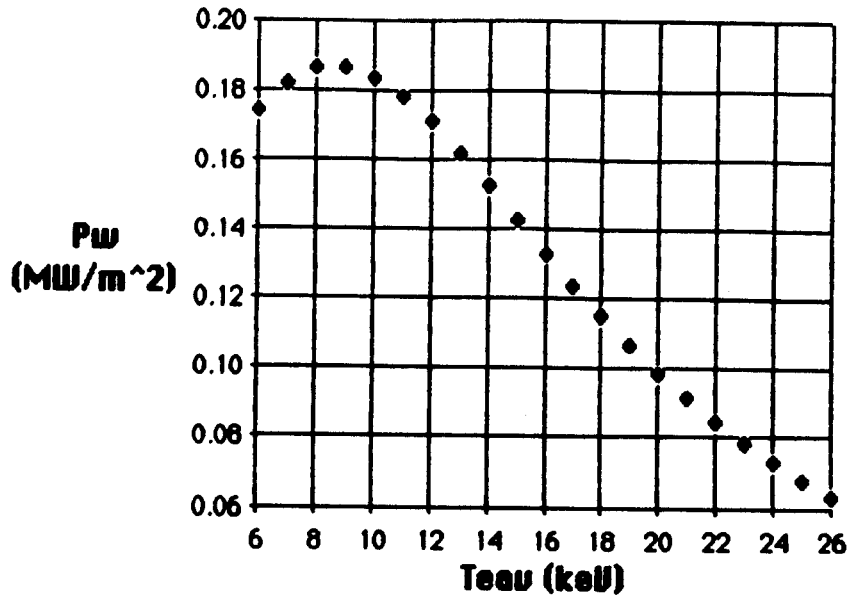


Figure 9
Neutron Wall Loading (MW/m²) vs. Average Temperature (keV)

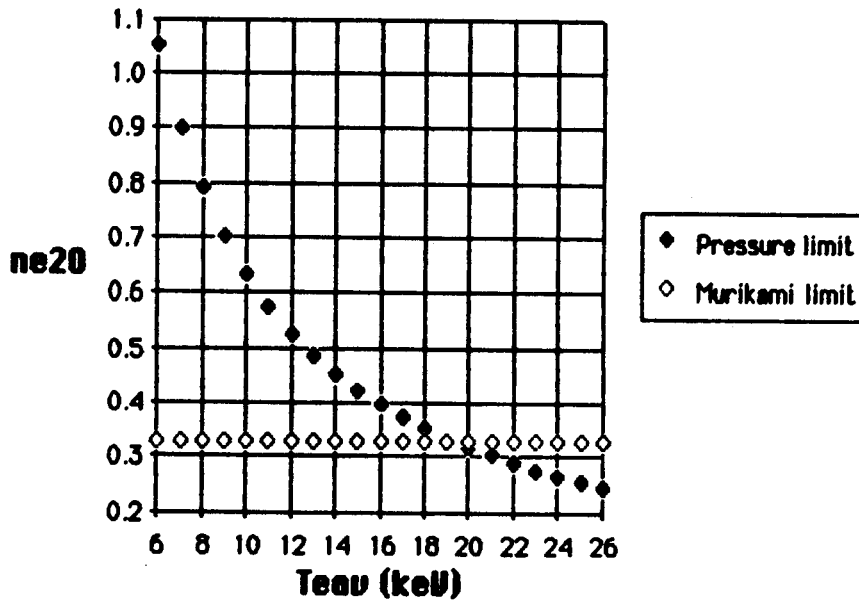


Figure 10
Average Electron Density (10²⁰/m³) vs. Average Electron Temperature (keV)

R_0 -2.96 m, a -1.25 m, B_t -3.45 T, κ -1.6
 q_{lim} -4.8, I_p -4.67 MA, β_{av} -4.0 %

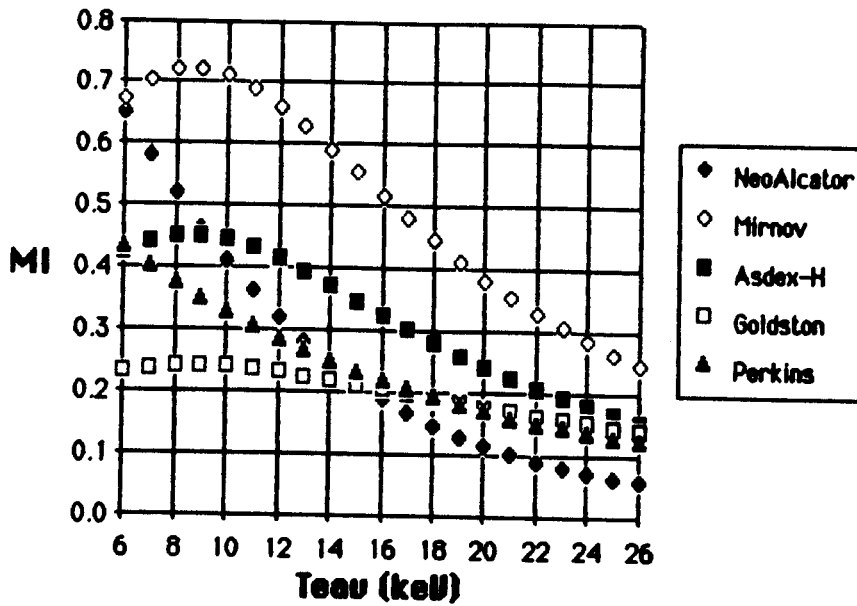


Figure 11
Ignition Margins vs. Average Electron Temperature (keV)

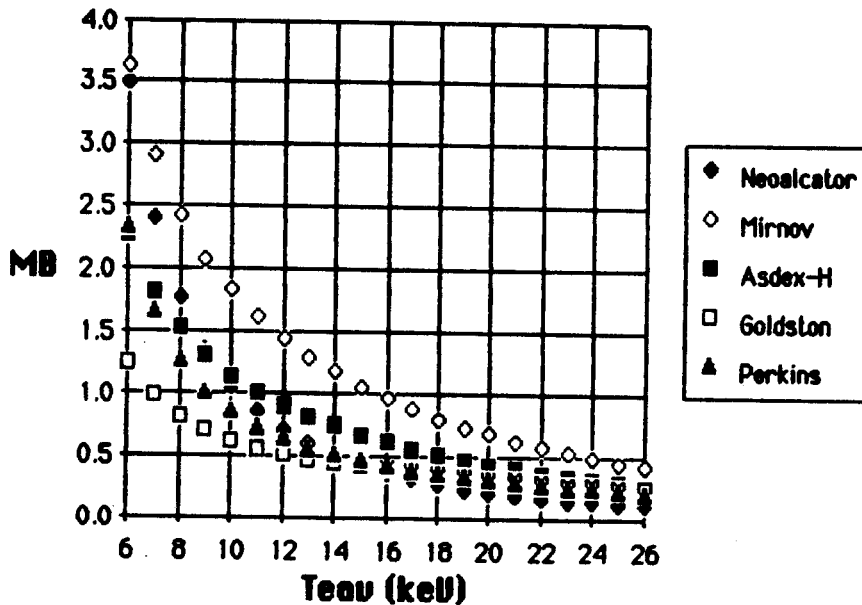


Figure 12
Burn Margins vs. Average Electron Temperature (keV)

R_o -2.96 m, a -1.25 m, B_t -3.45 T, κ -1.6
 q_{lim} -4.8, I_p -4.67 MA, β_{av} -4.0 %

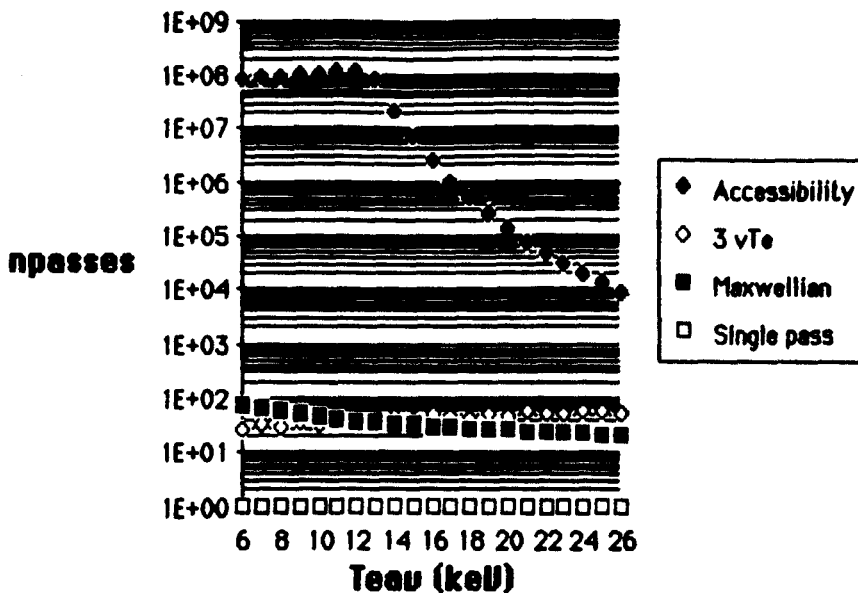


Figure 13
Number of passes for fast wave absorption vs. Average Electron Temperature (keV)

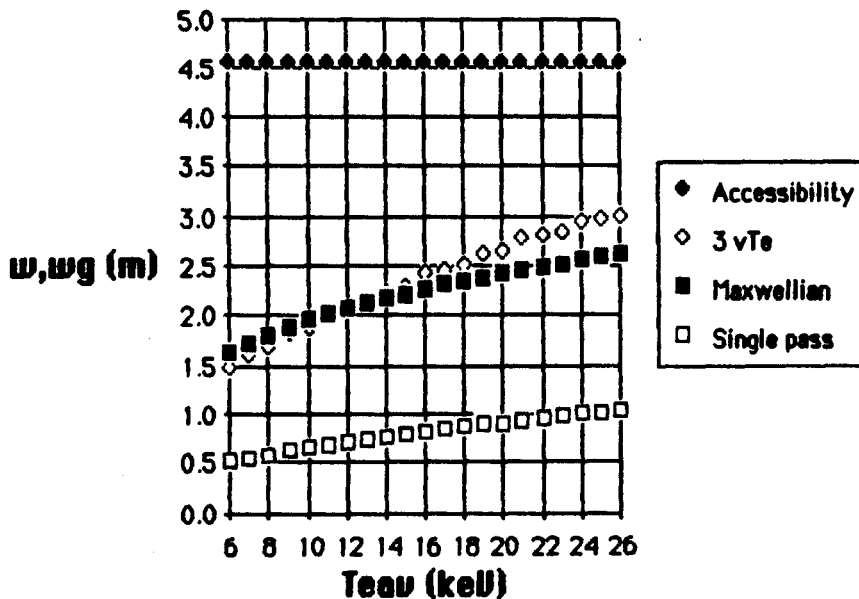


Figure 14
Width of waveguide array (4 element, 90° phasing) vs. Average Electron Temperature (keV)

$R_0 - 2.96 \text{ m}$, $a - 1.25 \text{ m}$, $B_t - 3.45 \text{ T}$, $\kappa - 1.6$
 $q_{lim} - 4.8$, $I_p - 4.67 \text{ MA}$, $\beta_{av} - 4.0 \%$

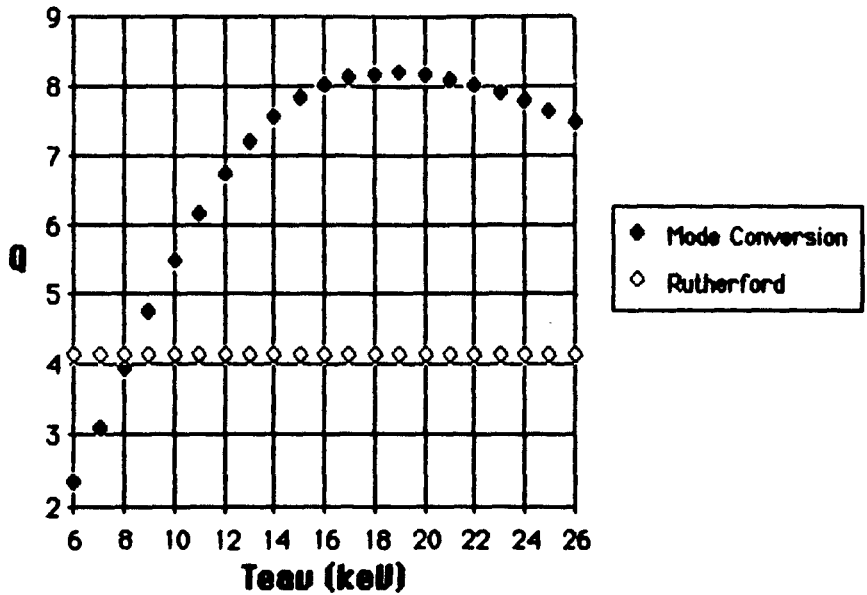


Figure 15
Slow Wave Lower Hybrid Q vs. Average Electron Temperature (keV)

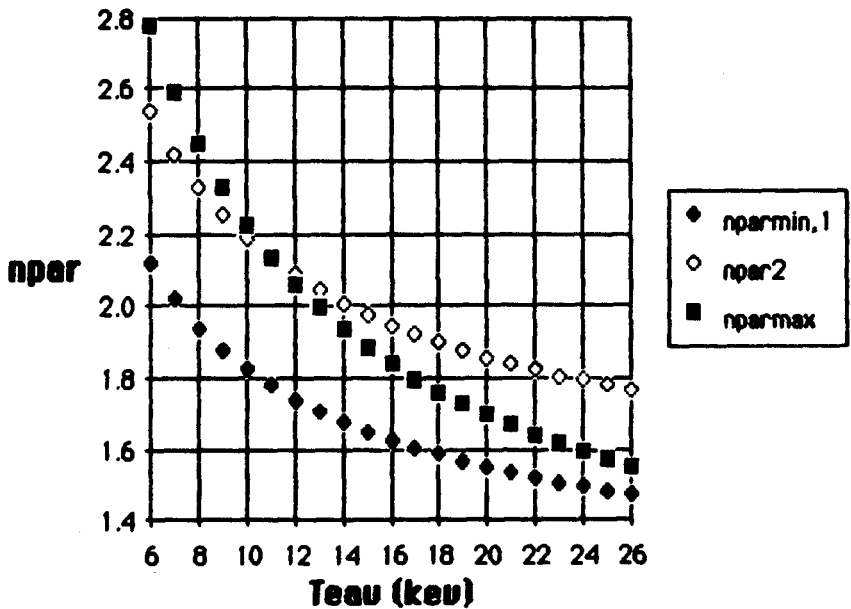


Figure 16
Parallel Indices of Refraction, Slow Wave vs. Average Electron Temperature (keV)

JULIET

R_0 -2.73 m, a -0.745 m, κ -2.16, B_t -5.0 T
 q_{lim} -2.2, I_p -10 MA, β_{av} -10.4 %

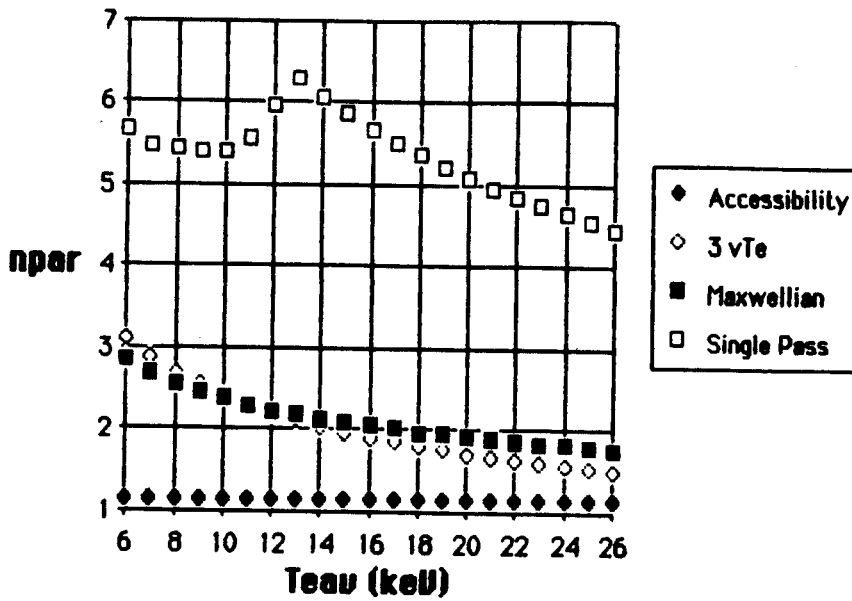


Figure 17
Parallel Indices of Refraction vs. Average Electron Temperature (keV)

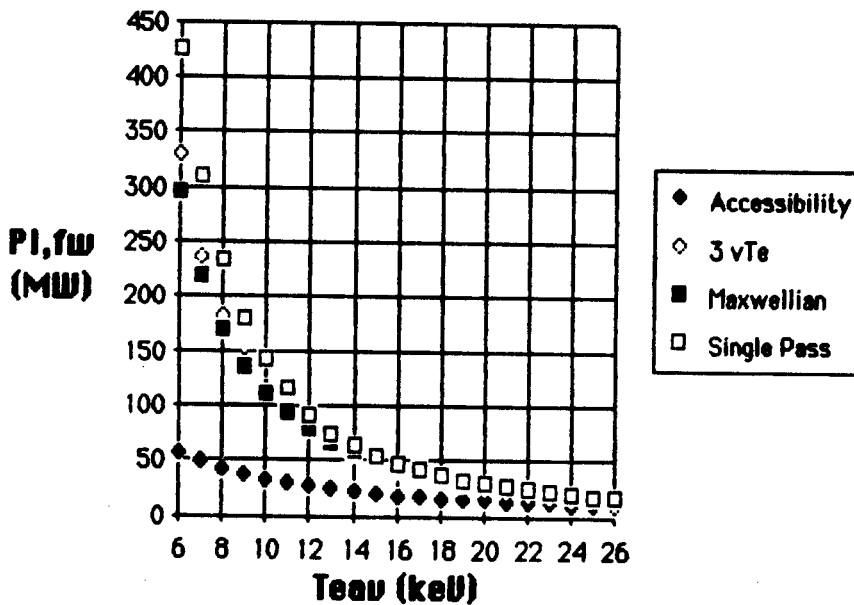


Figure 18
Required Fast Wave Power, no alphas (MW) vs. Temperature (keV)

FIRE

R_o -2.73 m, a -0.745 m, κ -2.16, B_t -5.0 T

q_{lim} -2.2, I_p -10 MA, β_{av} -10.4 %

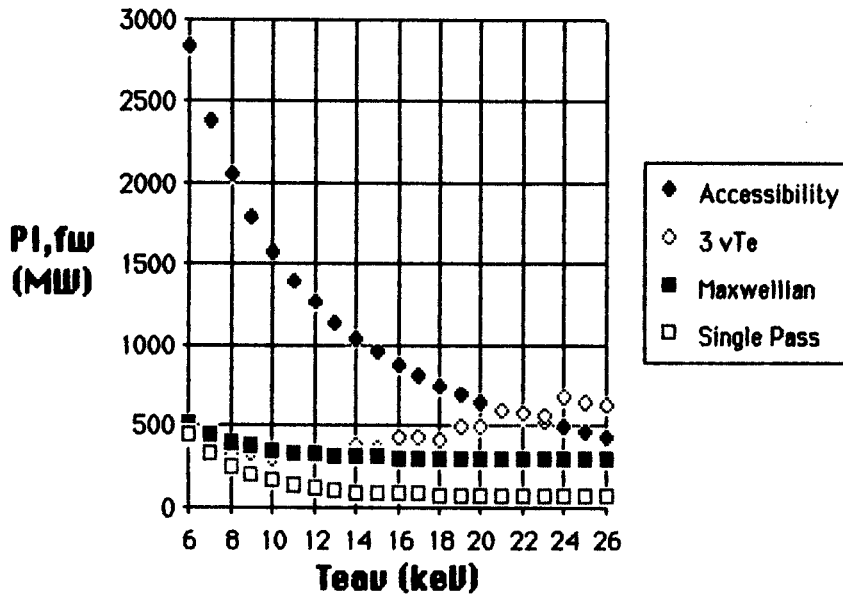


Figure 19
Required Fast Wave Power, with alphas (MW) vs. Temperature (keV)

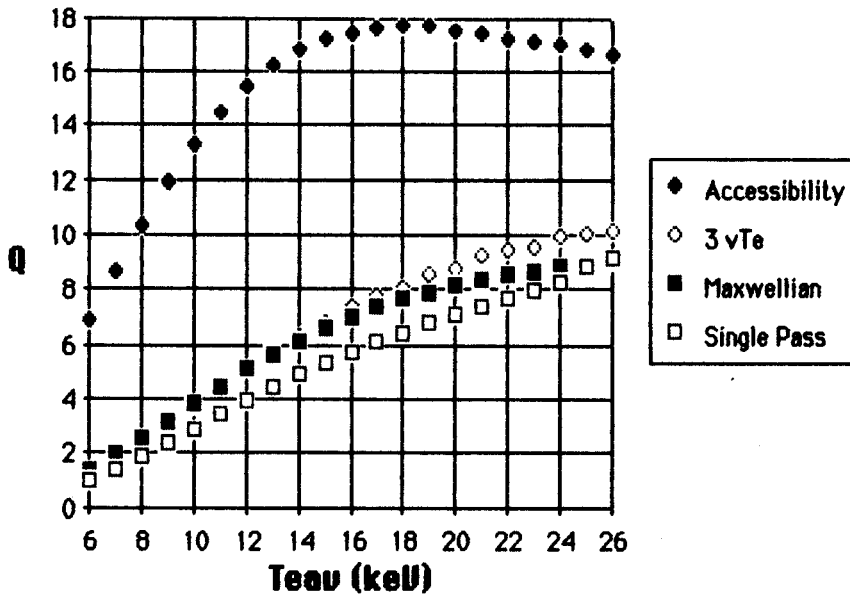


Figure 20
Q of Fast Wave Current Drive, no alphas vs. Average Temperature (keV)

$R_0 = 2.73 \text{ m}$, $a = 0.745 \text{ m}$, $\kappa = 2.16$, $B_t = 5.0 \text{ T}$

$q_{lim} = 2.2$, $I_p = 10 \text{ MA}$, $\beta_{av} = 10.4 \%$

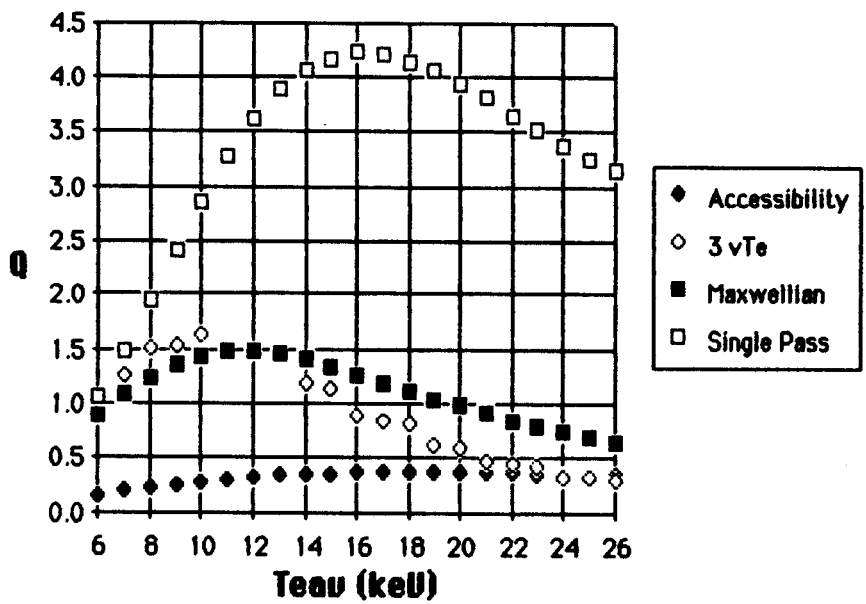


Figure 21

Q of Fast Wave Current Drive, with alphas vs. Temperature (keV)

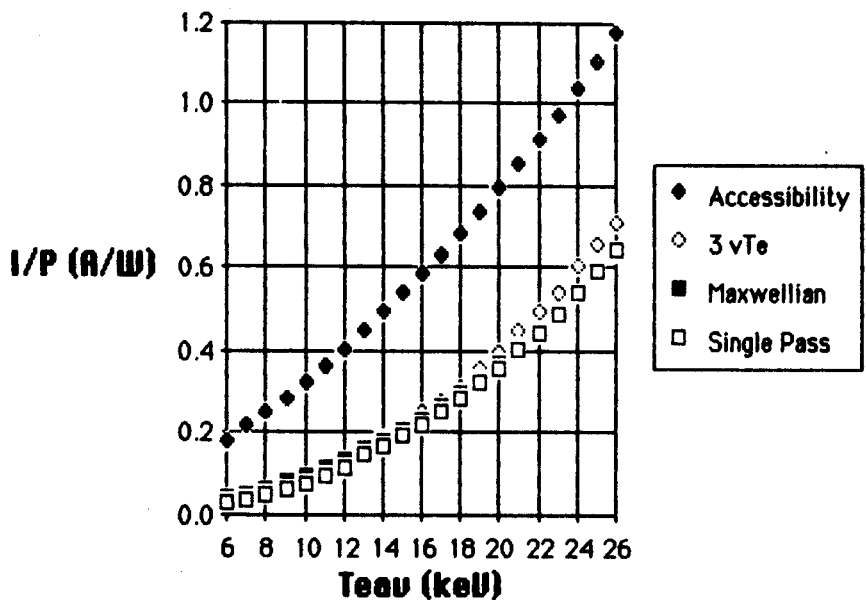


Figure 22

Fast wave I/P, no alphas vs. Average Temperature (keV)

NUMBER

R_0 -2.73 m, a -0.745 m, κ -2.16, B_t -5.0 T

q_{lim} -2.2, I_p -10 MA, β_{av} -10.4 %

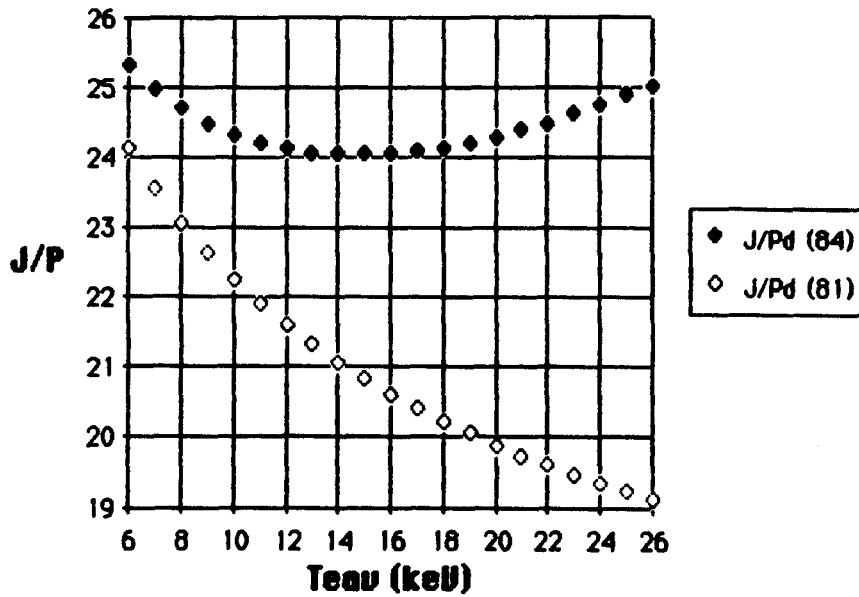


Figure 23
Normalized J/P (Karney/Fisch, 1984, Fisch/Karney, 1981)
Maxwellian tail, no alphas
vs. Average Electron Temperature (keV)

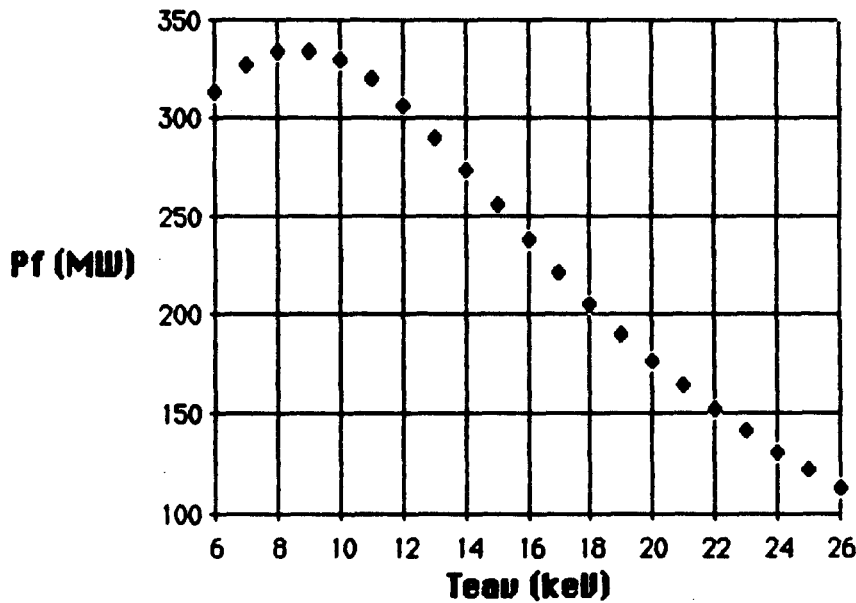


Figure 24
Fusion Power (MW) vs. Average Electron Temperature (keV)

TUBER

R_o -2.73 m, a -0.745 m, κ -2.16, B_t -5.0 T
 q_{lim} -2.2, I_p -10 MA, β_{av} -10.4 %

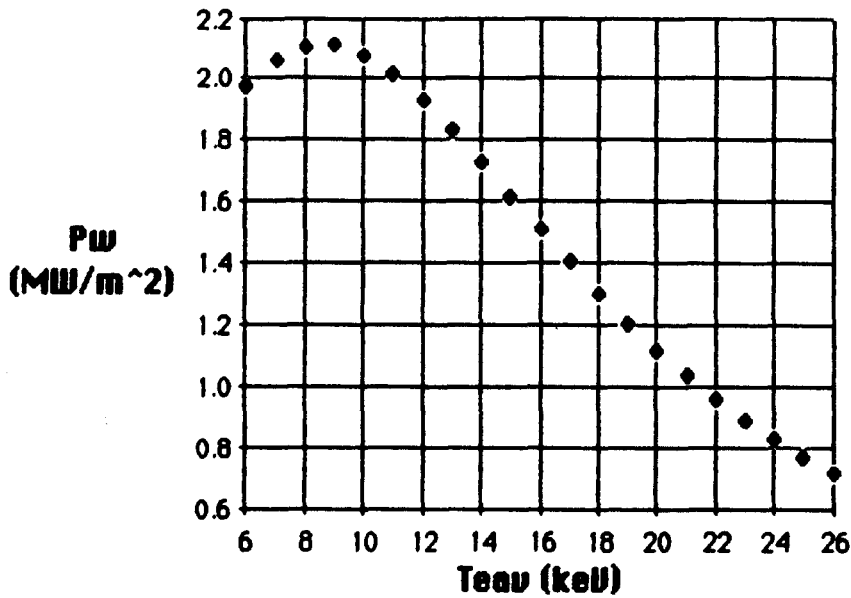


Figure 25
Neutron Wall Loading (MW/m²) vs. Average Temperature (keV)

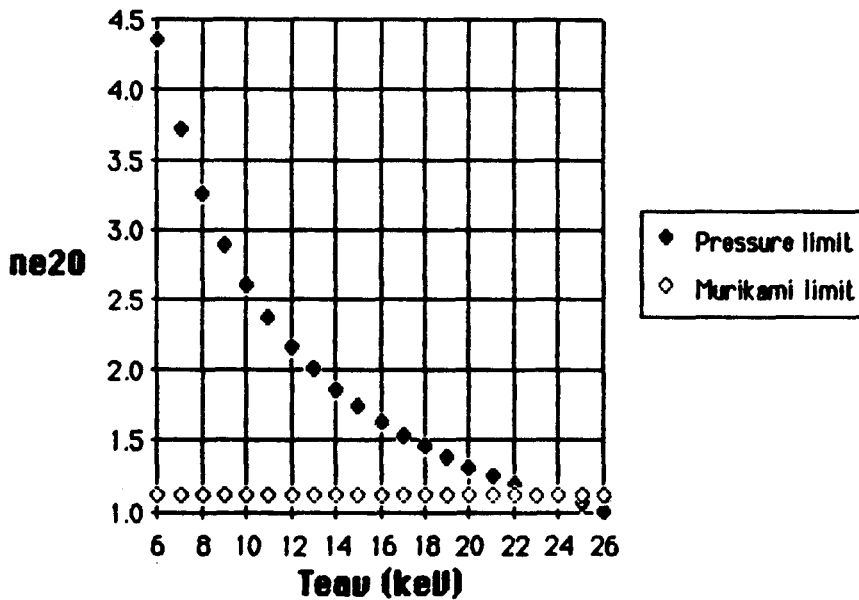


Figure 26
Average Electron Density (10²⁰/m³) vs. Average Electron Temperature (keV)

MI

$R_0 - 2.73 \text{ m}$, $a - 0.745$, $\kappa - 2.16$, $B_t - 5.0 \text{ T}$

$q_{lim} - 2.2$, $I_p - 10 \text{ MA}$, $\beta_{av} - 10.4 \%$

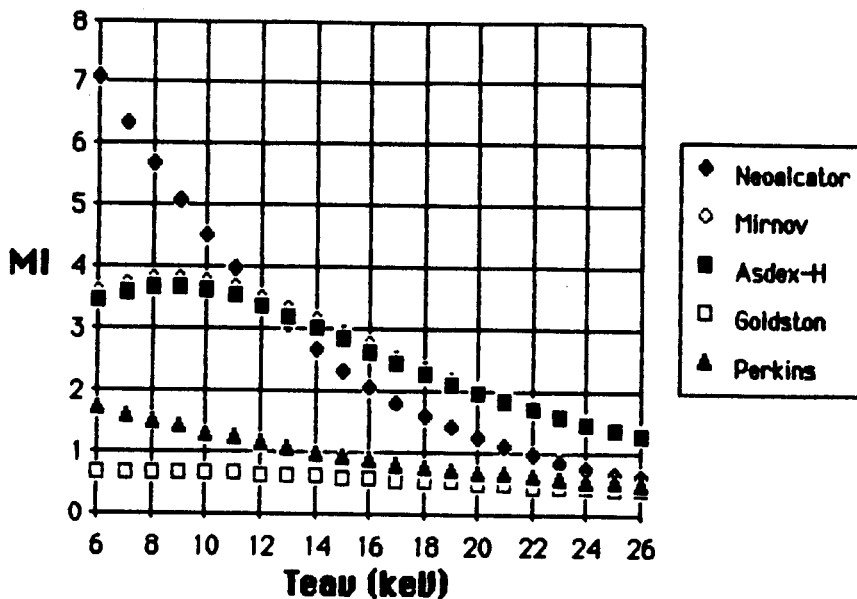


Figure 27
Ignition Margins vs. Electron Temperature (keV)

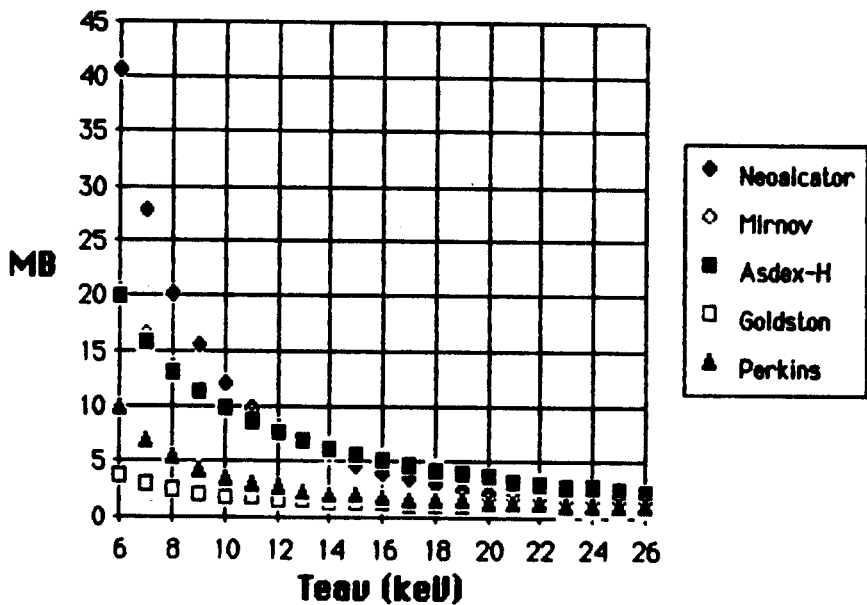


Figure 28
Burn Margins vs. Electron Temperature (keV)

TABLE

$R_0 - 2.73 \text{ m}$, $a - 0.745 \text{ m}$, $\kappa - 2.16$, $B_t - 5.0 \text{ T}$
 $q_{lim} - 2.2$, $I_p - 10 \text{ MA}$, $\beta_{av} - 10.4 \%$

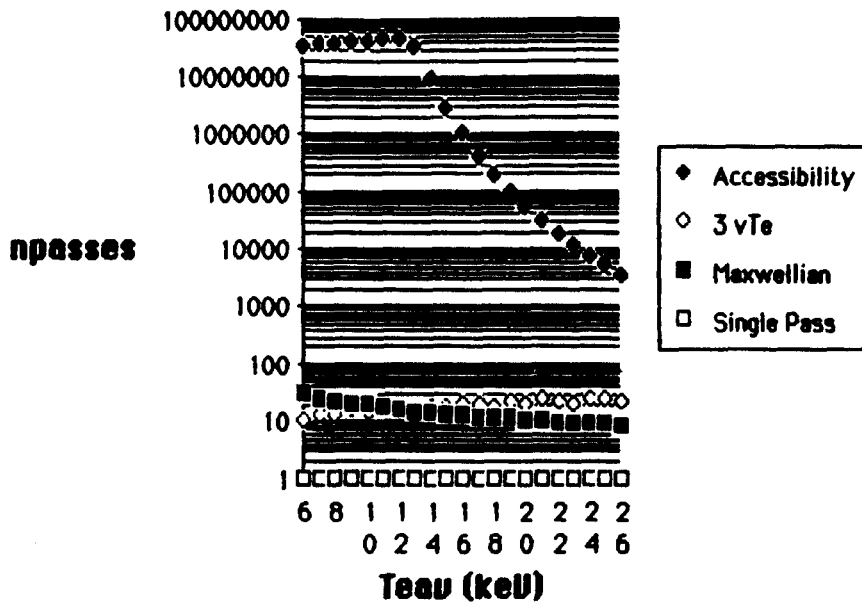


Figure 29
Number of passes for fast wave absorption
vs. Average Electron Temperature (keV)

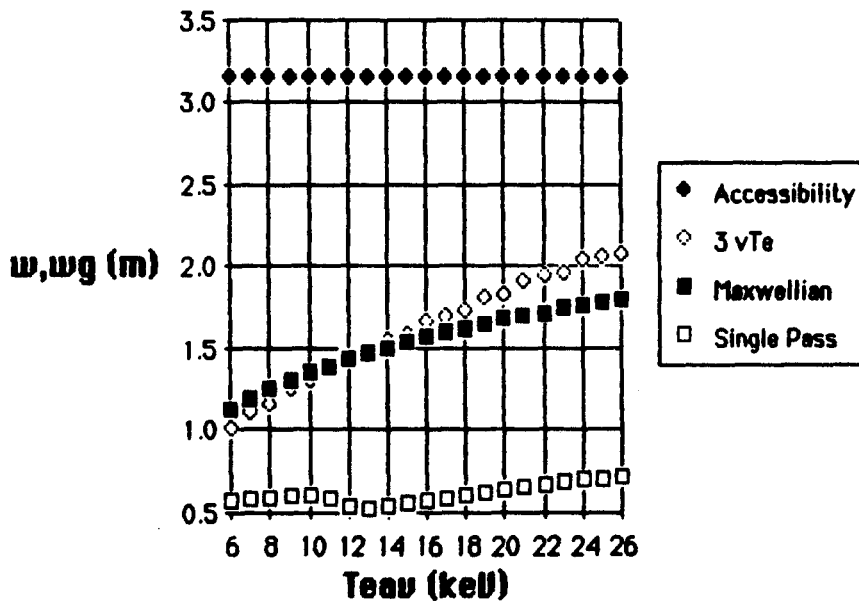


Figure 30
Width of waveguide array (4 element, 90° phasing)
vs. Average Electron Temperature (keV)

TUBER

R_o -2.73 m, a -0.745 m, κ -2.16, B_t -5.0 T
 q_{lim} -2.2, I_p -10 MA, β_{av} -10.4 %

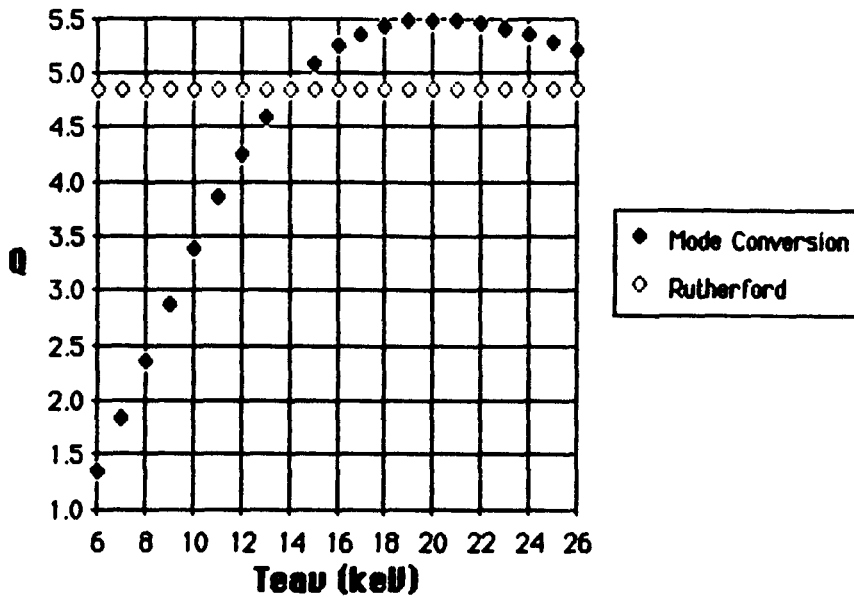


Figure 31
Slow Wave Lower Hybrid Q vs. Average Electron Temperature (keV)

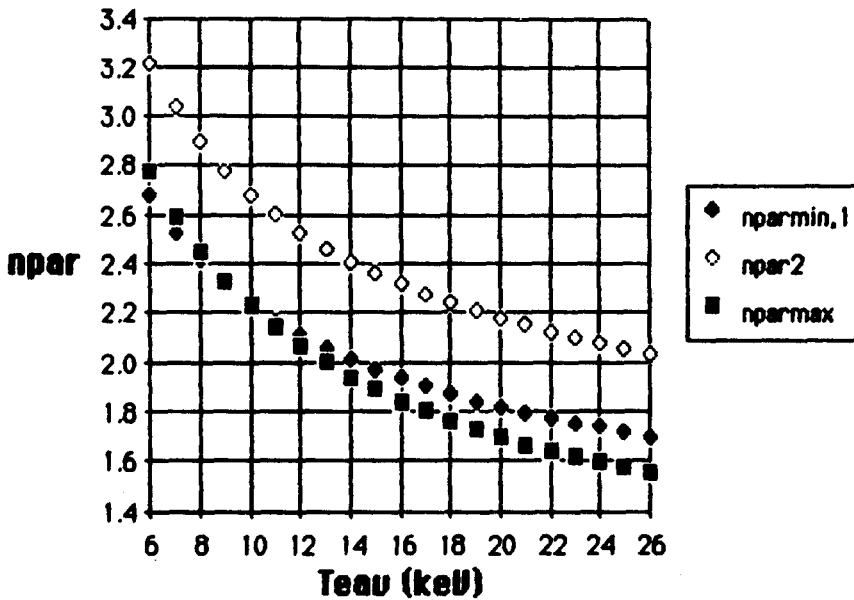


Figure 32
Parallel Indices of Refraction, Slow Wave vs. Average Electron Temperature (keV)

Magic5

**R_0 -3.95 m, a -0.79 m, B_t -6.88 T, κ -1.6,
 q_{lim} -2.1, I_p -5.42 MA, β_{av} -3.6 %**

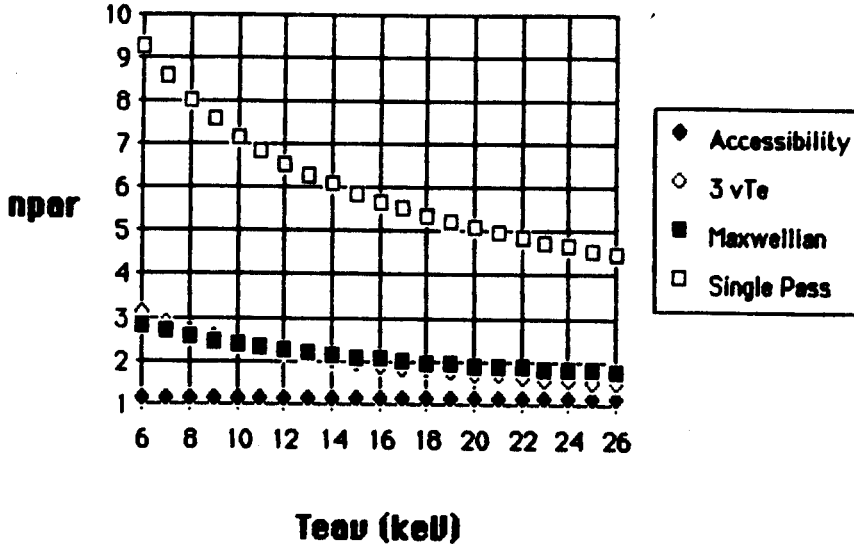


Figure 33
Parallel Indices of Refraction vs. Average Temperature (keV)

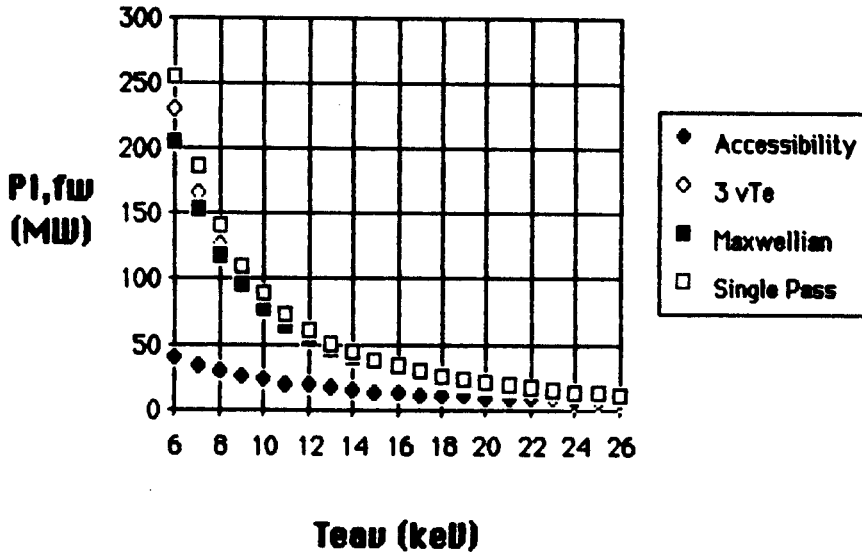


Figure 34
Required Fast Wave Power, no alphas (MW) vs. Temperature (keV)

Magic5

$R_0=3.95$ m, $a=0.79$ m, $B_t=6.88$ T, $\kappa=1.6$,

$q_{lim}=2.1$, $I_p=5.42$ MA, $\beta_{av}=3.6\%$

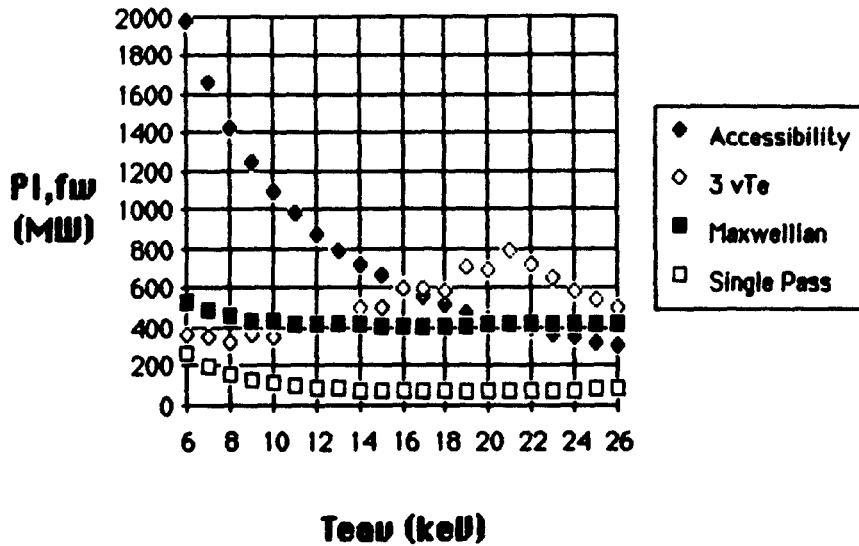


Figure 35
Required Fast Wave Power, with alphas (MW) vs. Temperature (keV)

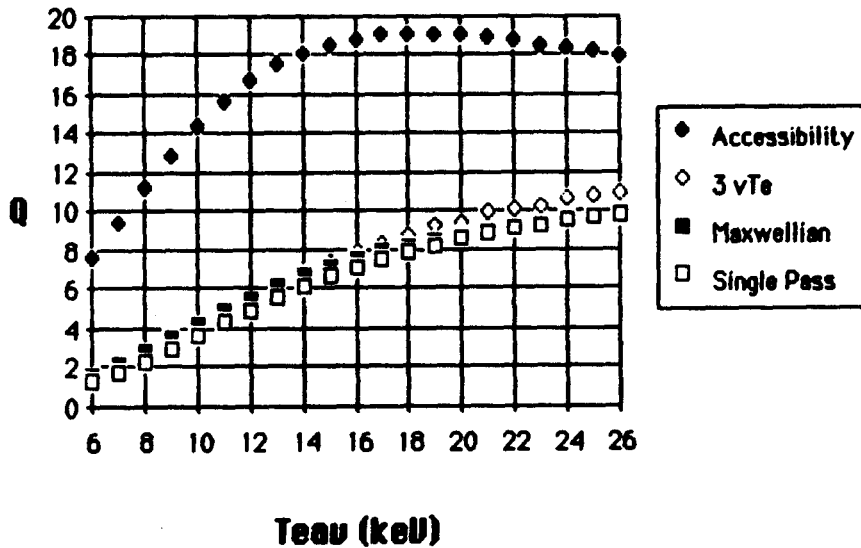


Figure 36
Q of Fast Wave Current Drive, no alphas vs. Average Temperature (keV)

Magic5

**R_0 -3.95 m, a -0.79 m, B_t -6.88 T, κ -1.6,
 q_{lim} -2.1, I_p -5.42 MA, β_{av} -3.6 %**

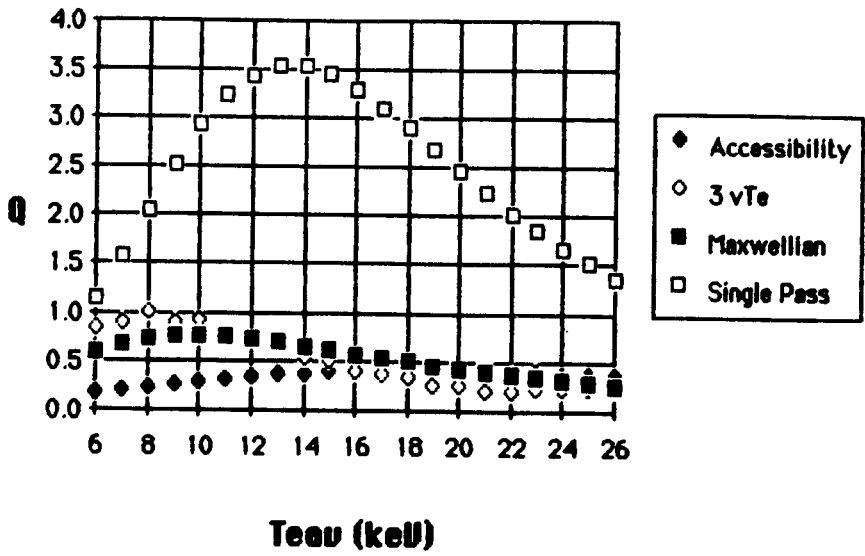


Figure 37
Hypothetical Q of Fast Wave Current Drive, with alphas
vs. Average Temperature (keV)

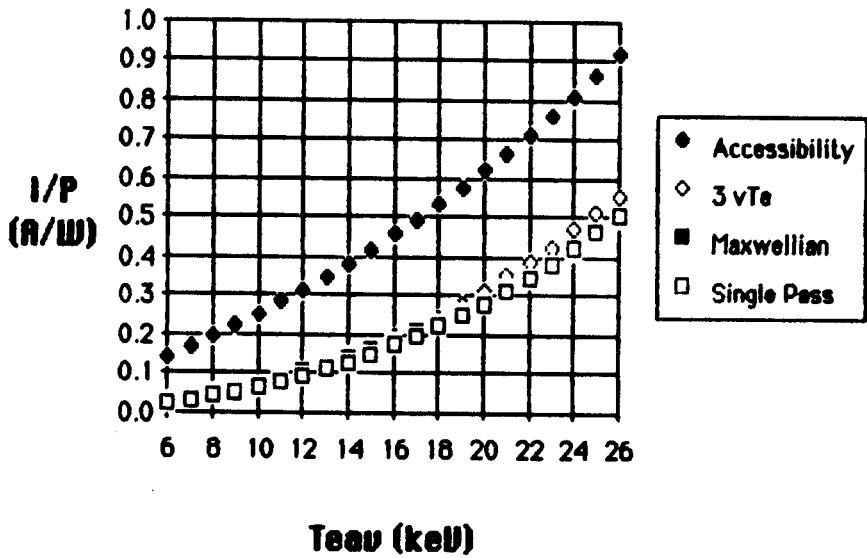


Figure 38
Fast Wave I/P (A/W), no alphas vs. Average Temperature (keV)

Magic5

$R_0 = 3.95 \text{ m}$, $a = 0.79 \text{ m}$, $B_t = 6.88 \text{ T}$, $\kappa = 1.6$,
 $q_{lim} = 2.1$, $I_p = 5.42 \text{ MA}$, $\beta_{av} = 3.6 \%$

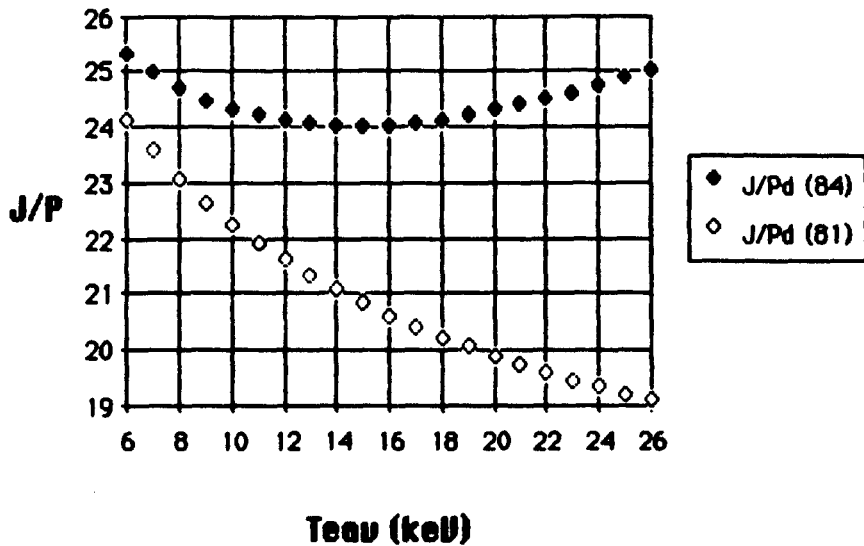


Figure 39
Normalized J/P (Karney/Fisch, 1984; Fisch/Karney, 1981)
Maxwellian Tail, no alphas
vs. Average Electron Temperature

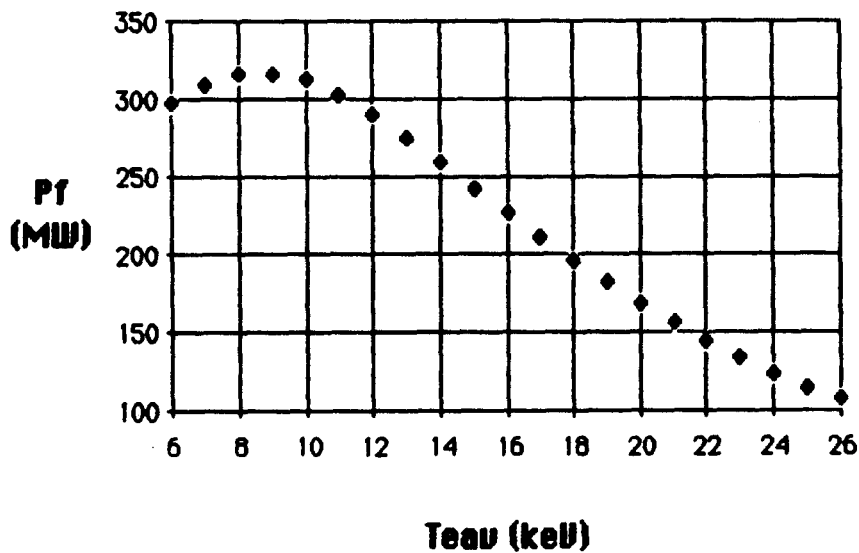


Figure 40
Fusion Power (MW) vs. Average Electron Temperature (keV)

Magic5

$R_0=3.95$ m, $a=0.79$ m, $B_t=6.88$ T, $\kappa=1.6$,
 $q_{lim}=2.1$, $I_p=5.42$ MA, $\beta_{av}=3.6$ %

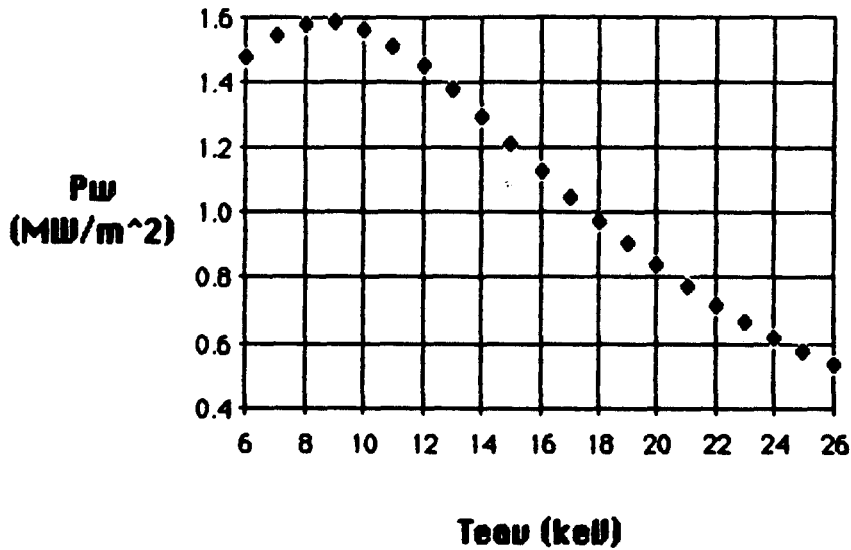


Figure 41
Neutron Wall Loading (MW/m^2)
vs. Average Electron Temperature (keV)

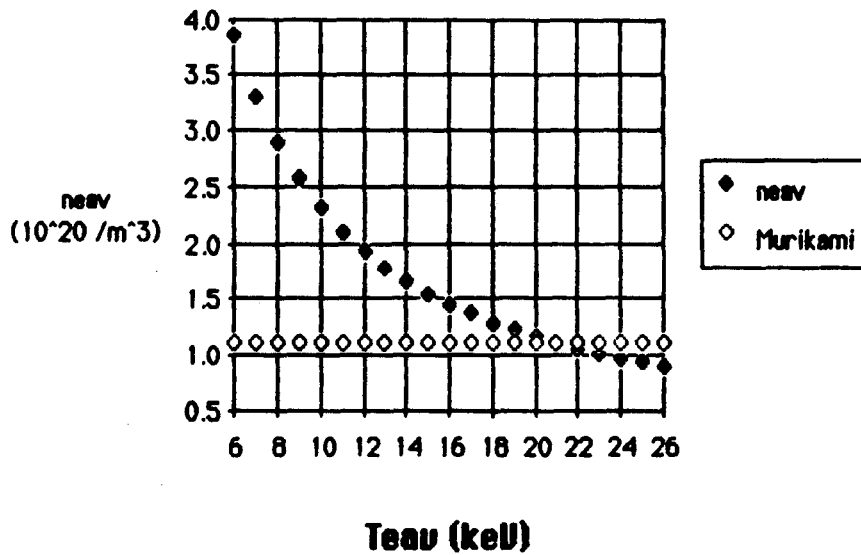


Figure 42
Average Electron Density ($10^{20}/m^3$)
vs. Average Electron Temperature (keV)

Magic5

R_0 -3.95 m, a -0.79 m, B_t -6.88 T, κ -1.6

q_{lim} -2.1, I_p -5.42 MA, β_{av} -3.6 %

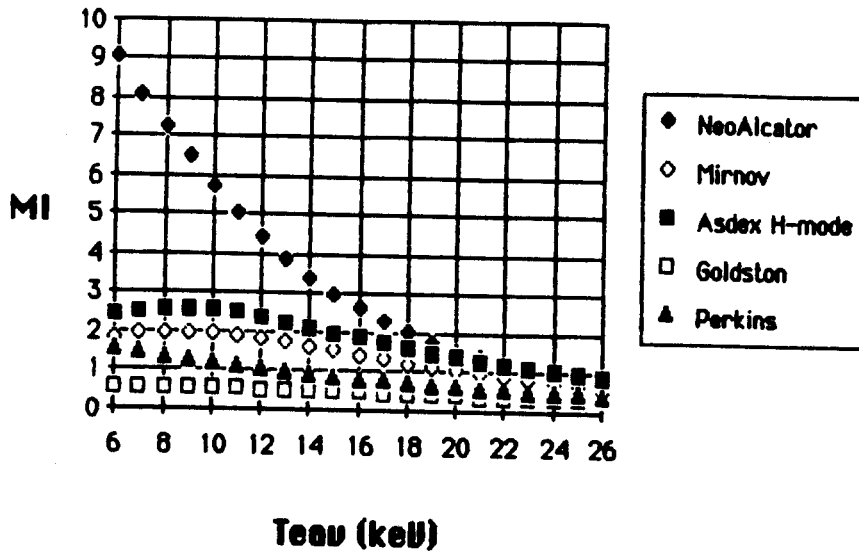


Figure 43
Ignition Margin vs. Average Temperature (keV)

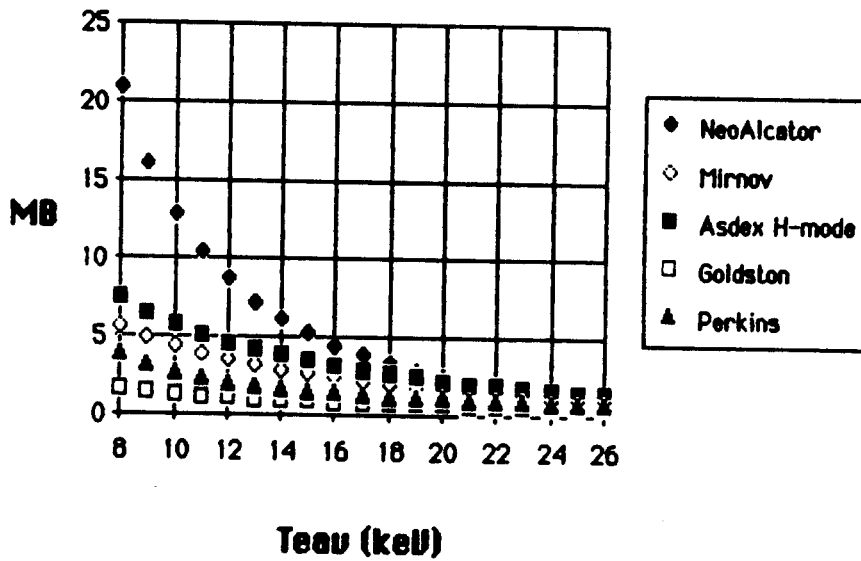


Figure 44
Burn Margins, Fast Wave Maxwellian, no alphas
vs. Average Electron Temperature (keV)

Magic5

R_0 -3.95 m, a -0.79 m, B_t -6.88 T, κ -1.6,
 q_{lim} -2.1, I_p -5.42 MA, β_{av} -3.6 %

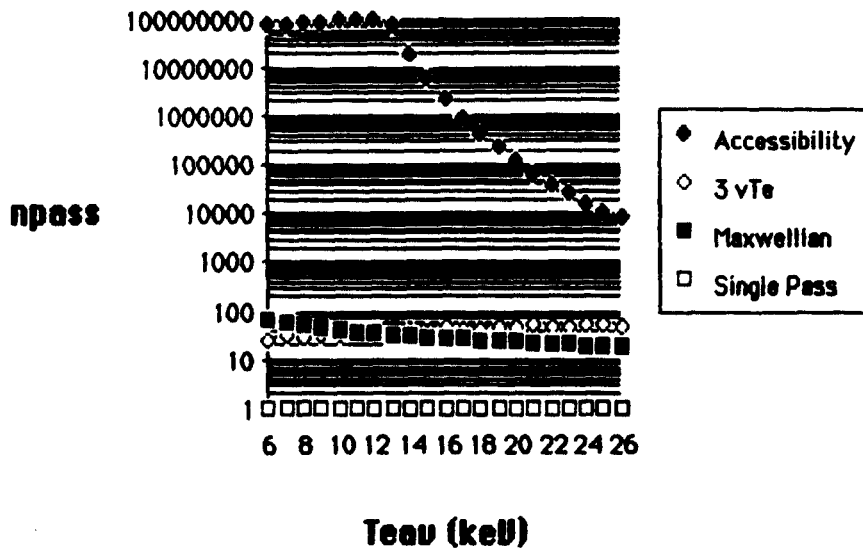


Figure 45
Number of passes for fast wave absorption
vs. Average Electron Temperature (keV)

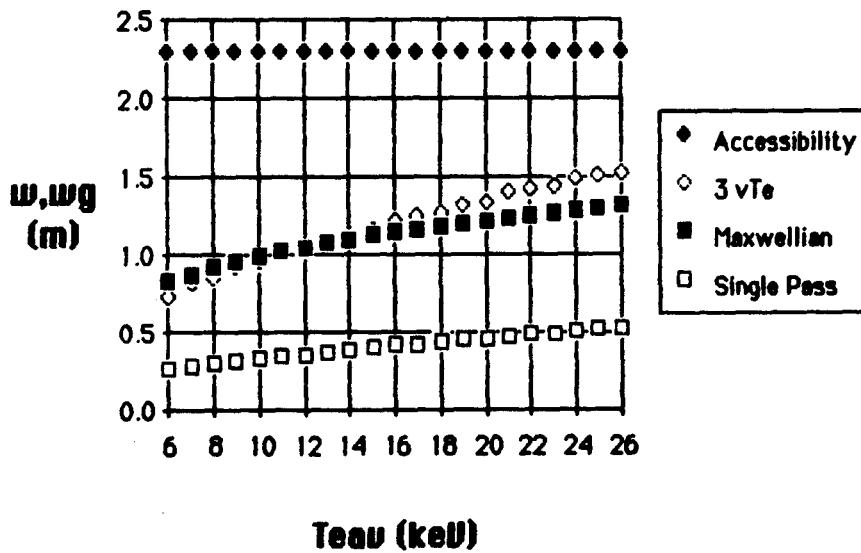


Figure 46
Width of wave guide array (4 element, 90° phasing)
vs. Average Electron Temperature (keV)

Magic5

$R_0=3.95$ m, $a=0.79$ m, $B_t=6.88$ T, $\kappa=1.6$,

$q_{lim}=2.1$, $I_p=5.42$ MA, $\beta_{av}=3.6$ %

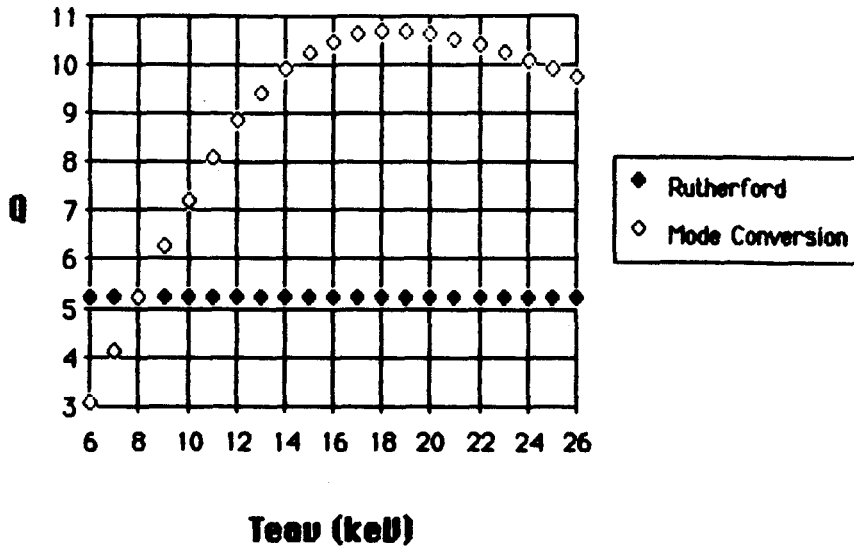


Figure 47
Slow Wave Lower Hybrid Q vs. Average Electron Temperature (keV)

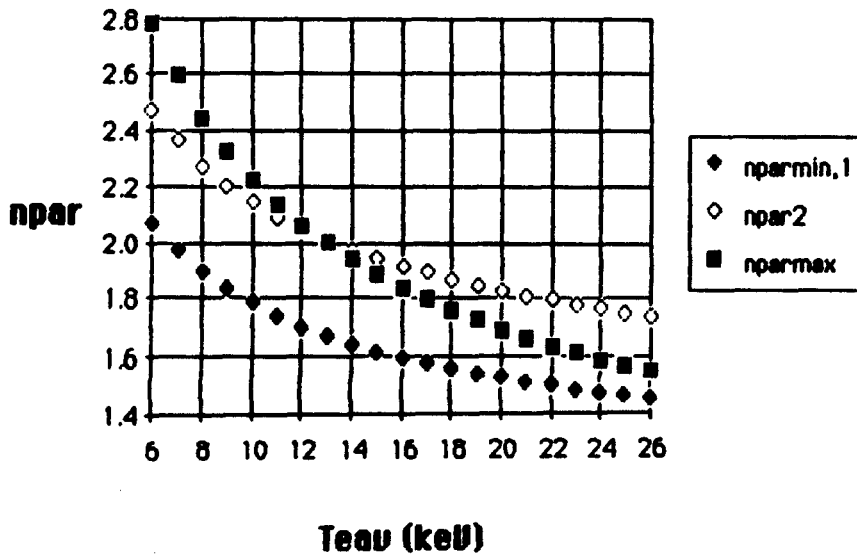


Figure 48
Parallel Indices of Refraction, Slow Wave vs. Average Electron Temperature (keV)

ET-0

**R_o -2.2 m, a -0.6 m, κ -10, I_p -14.9 MA
 B_t -2.1 T, q_{lim} -7.0, β_{av} -44 %**

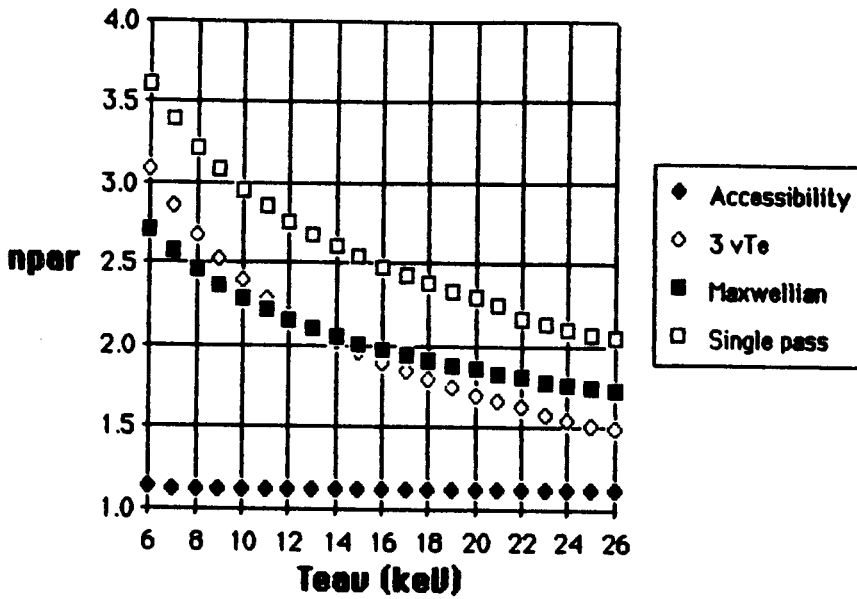


Figure 49

Parallel Indices of Refraction vs. Average Electron Temperature (keV)

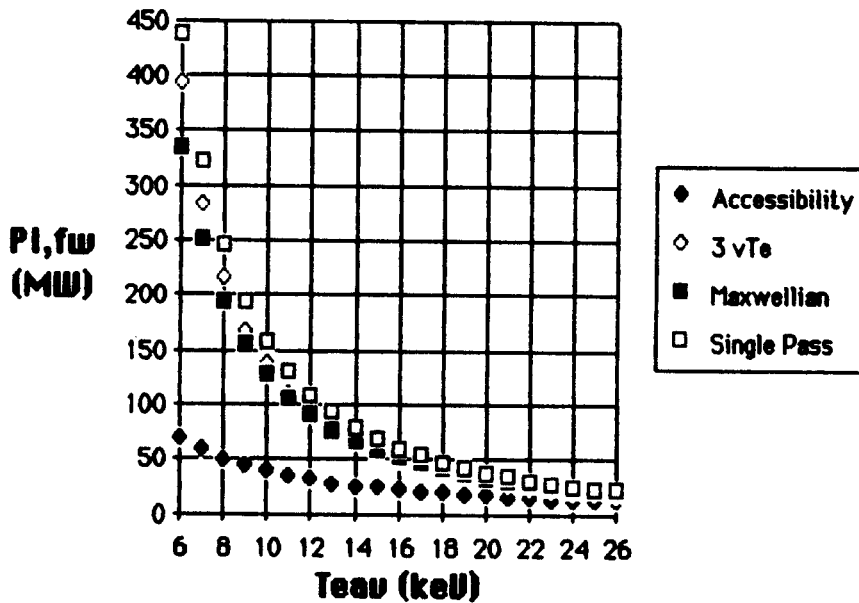


Figure 50

Required Fast Wave Power, no alphas (MW) vs. Temperature (keV)

ET-III

R_0 -2.2 m, a -0.6 m, κ -10, I_p -14.9 MA

B_t -2.1 T, q_{lim} -7.0, β_{av} -44 %

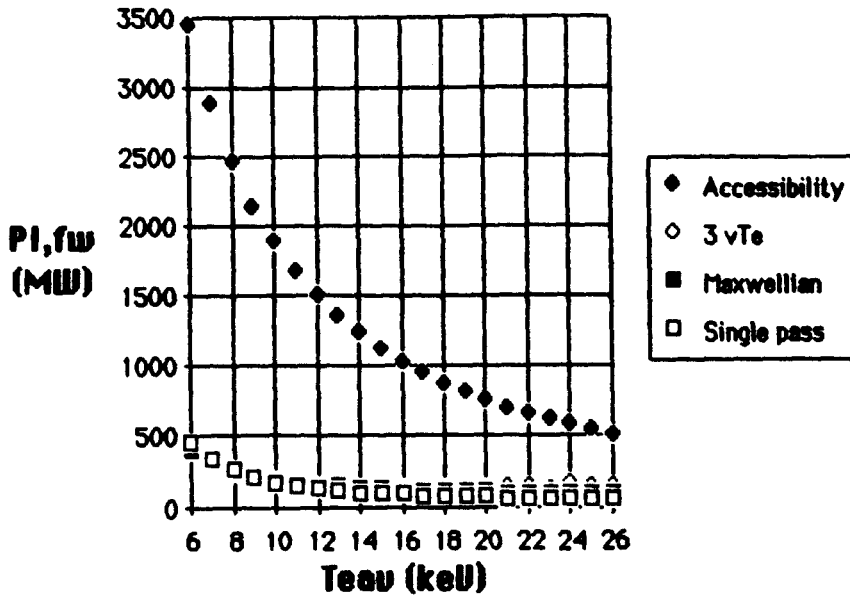


Figure 51

Required Fast Wave Power, with alphas (MW) vs. Temperature (keV)

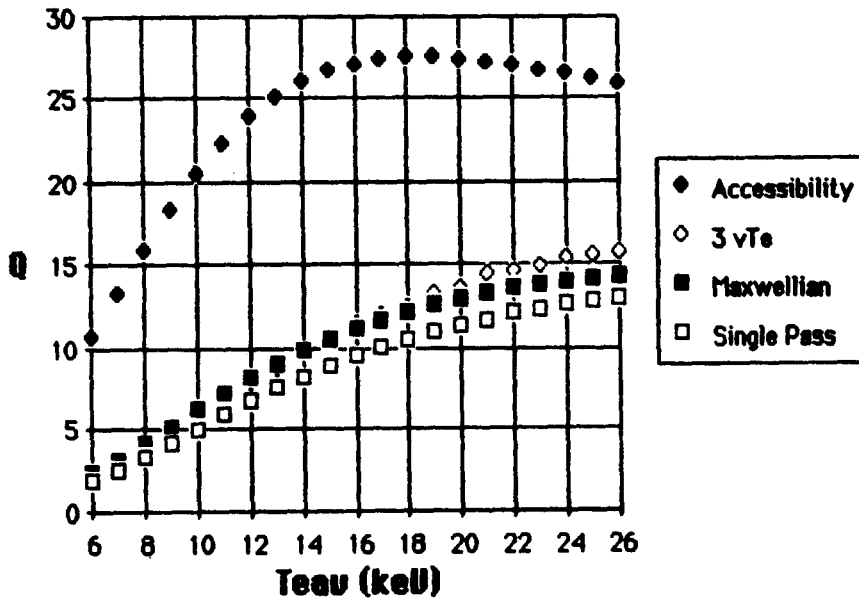


Figure 52

Q of Fast Wave Current Drive, no alphas vs. Temperature (keV)

ET-10

R_0 -2.2 m, a -0.6 m, κ -10, I_p -14.9 MA

B_t -2.1 T, q_{lim} -7.0, β_{av} -44 %

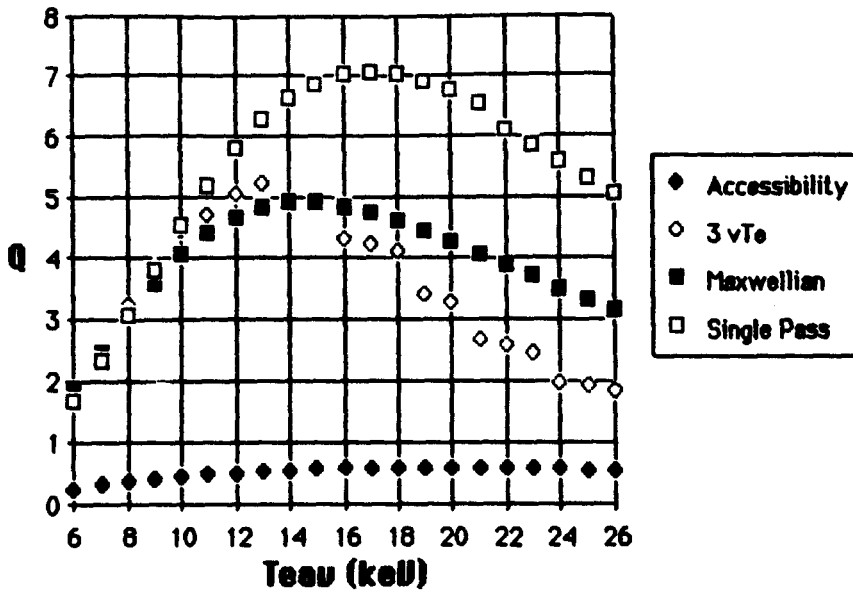


Figure 53

Q of Fast Wave Current Drive, with alphas vs. Temperature (keV)

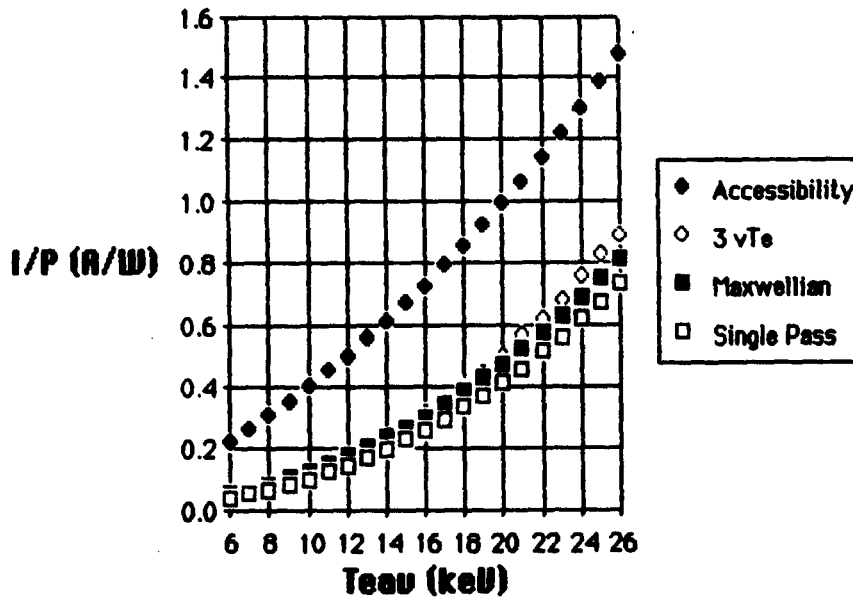


Figure 54

Fast Wave I/P, no alphas vs. Average Temperature (keV)

FT-10

R_0 -2.2 m, a -0.6 m, $kappa$ -10, I_p -14.9 MA

B_t -2.1 T, q_{lim} -7.0, $beta_{av}$ -44 %

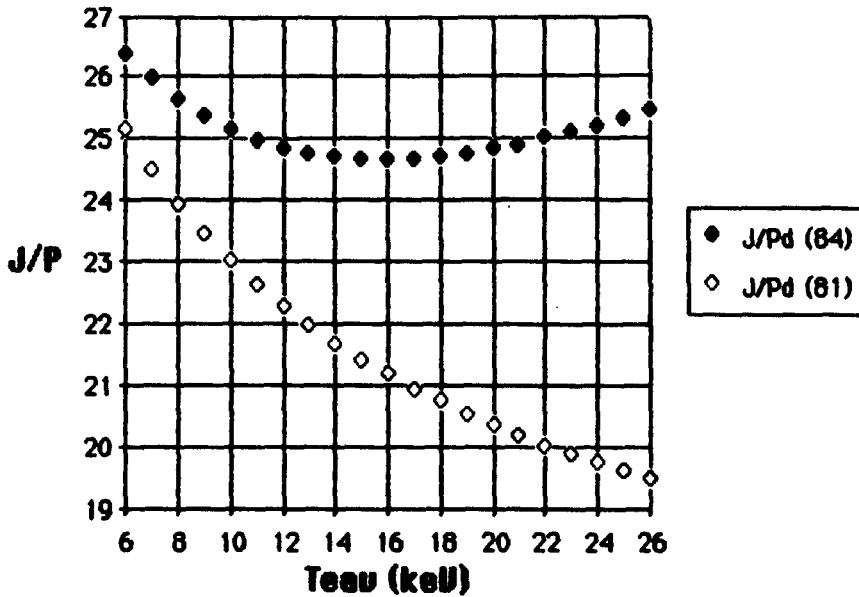


Figure 55

Normalized J/P (Karney/Fisch, 1984, Fisch/Karney, 1981)

Maxwellian Tail, no alphas

vs. Average Electron Temperature (keV)

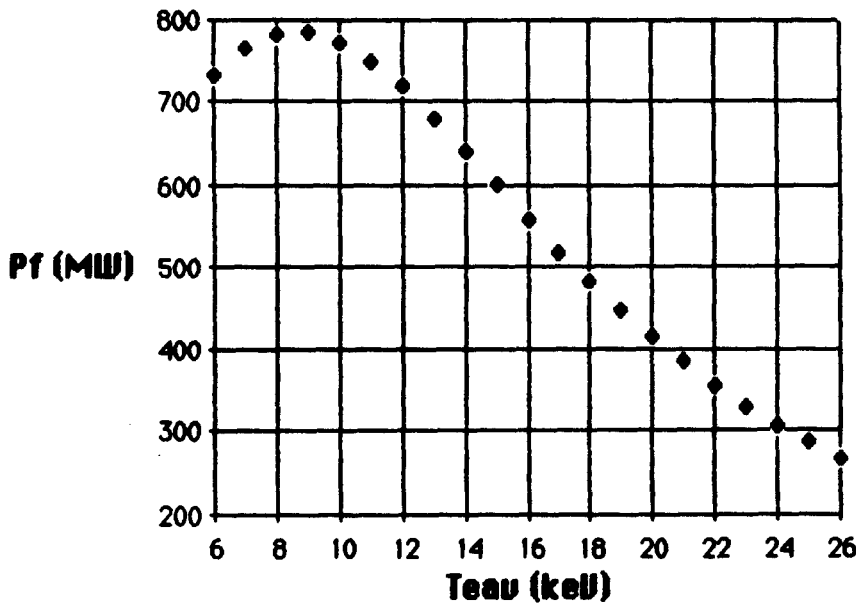


Figure 56

Fusion Power (MW) vs. Average Electron Temperature (keV)

R_0 -2.2 m, a -0.6 m, κ -10, I_p -14.9 MA
 B_t -2.1 T, q_{lim} -7.0, β_{av} -44 %

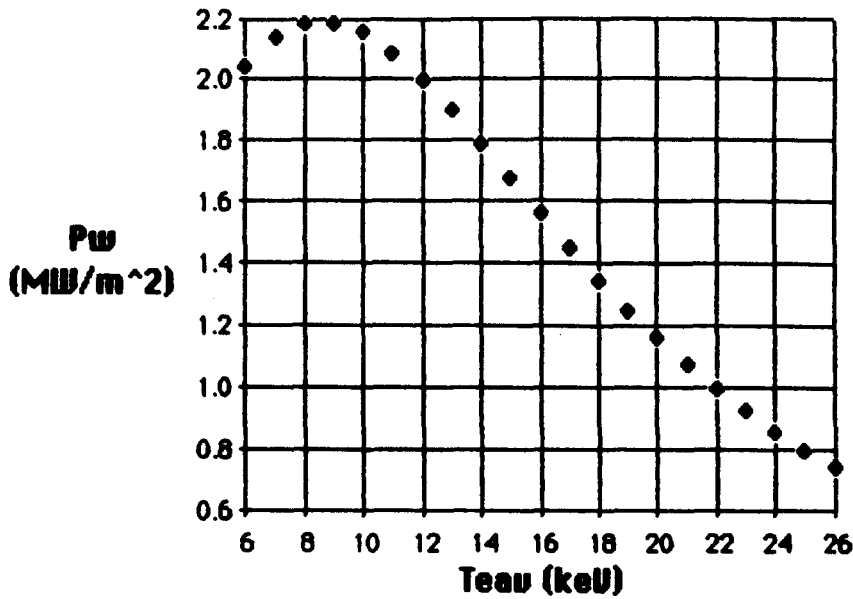


Figure 57
Neutron Wall Loading (MW/m²) vs. Average Temperature (keV)

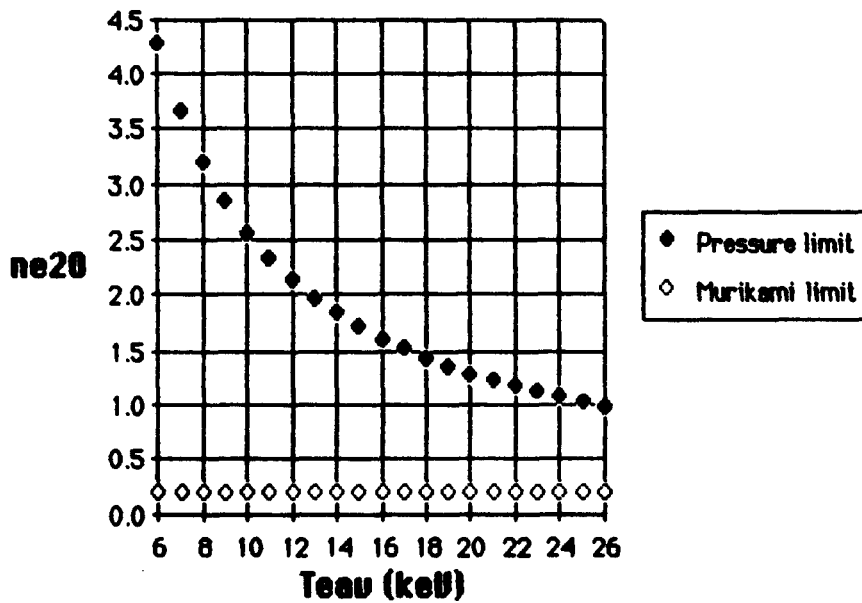


Figure 58
Average Electron Density (10²⁰/m³) vs. Average Electron Temperature (keV)

ET-II

R_0 -2.2 m, a -0.6 m, $kappa$ -10, I_p -14.9 MA

B_t -2.1 T, q_{lim} -7.0, $beta_{av}$ -44 %

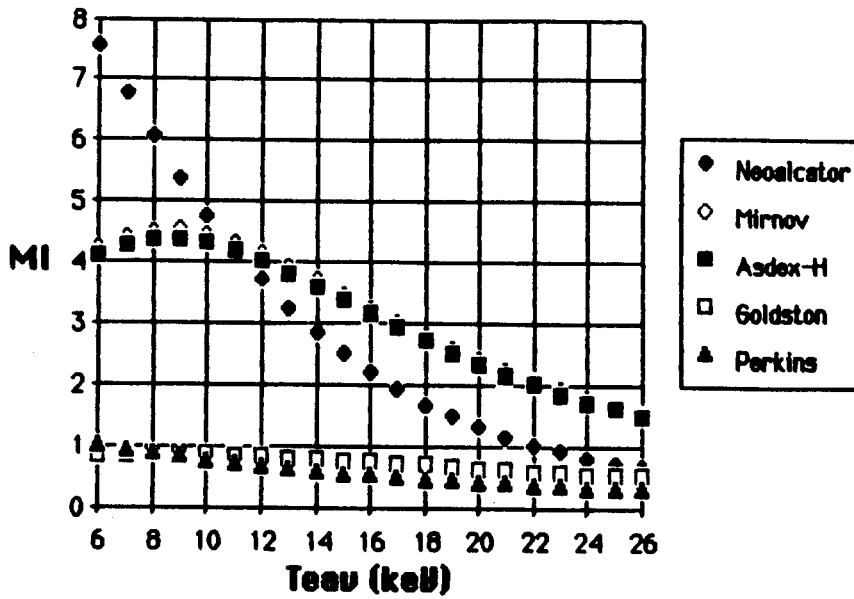


Figure 59
Ignition Margins vs. Electron Temperature (keV)

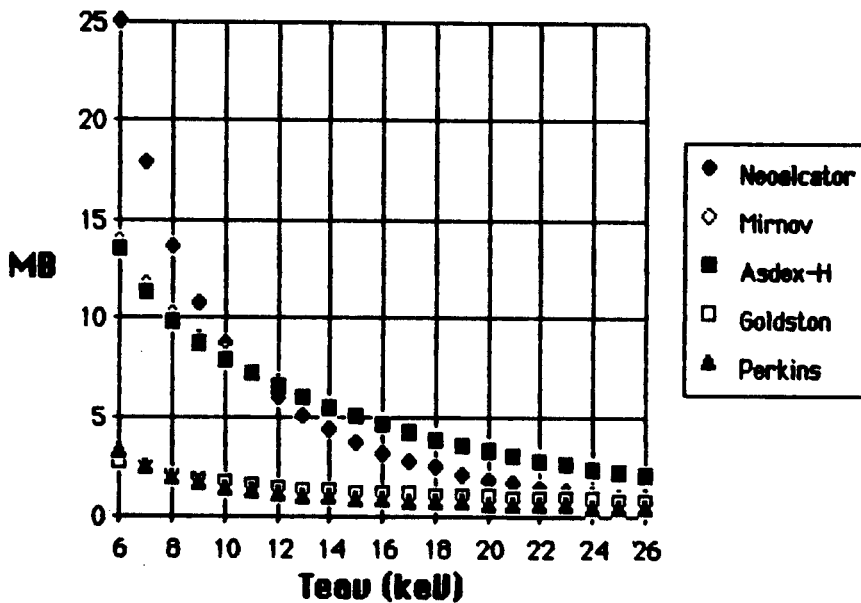


Figure 60
Burn Margins vs. Average Electron Temperature (keV)

R_o -2.2 m, a -0.6 m, κ -10, I_p -14.9 MA
 B_t -2.1 T, q_{lim} -7.0, β_{av} -44 %

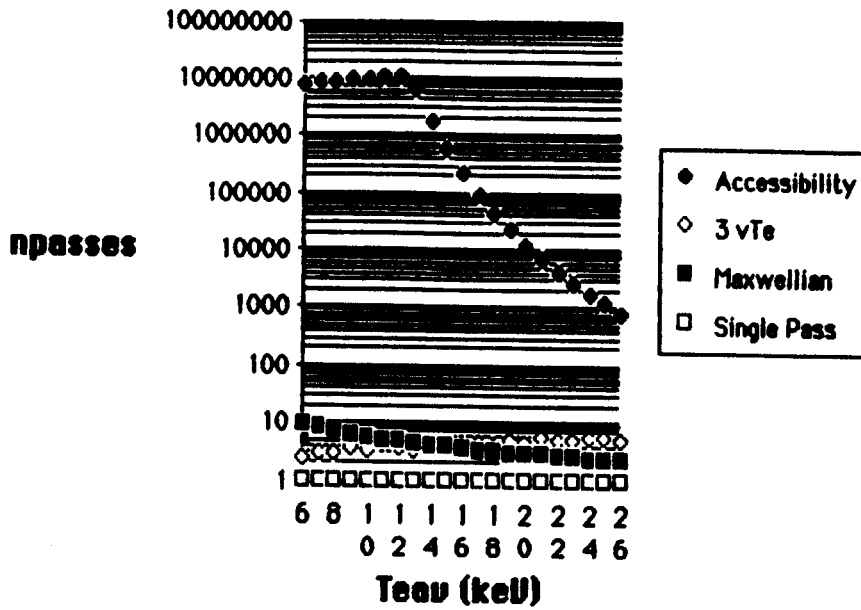


Figure 61
 Number of passes for fast wave absorption
 vs. Average Electron Temperature (keV)

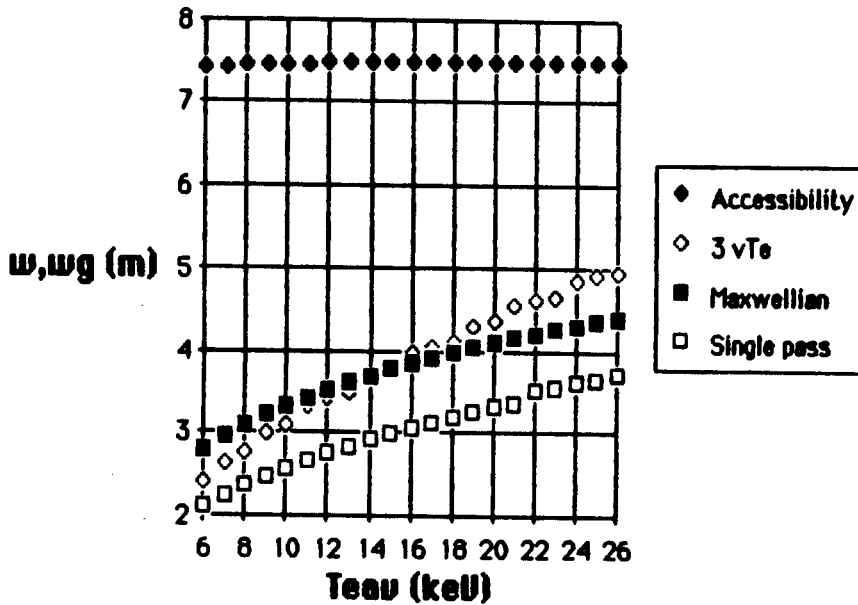


Figure 62
 Width of waveguide array (4 element, 90° phasing)
 vs. Average Electron Temperature (keV)

ET-II

R_0 -2.2 m, a -0.6 m, κ -10, I_p -14.9 MA

B_t -2.1 T, q_{lim} -7.0, β_{av} -44 %

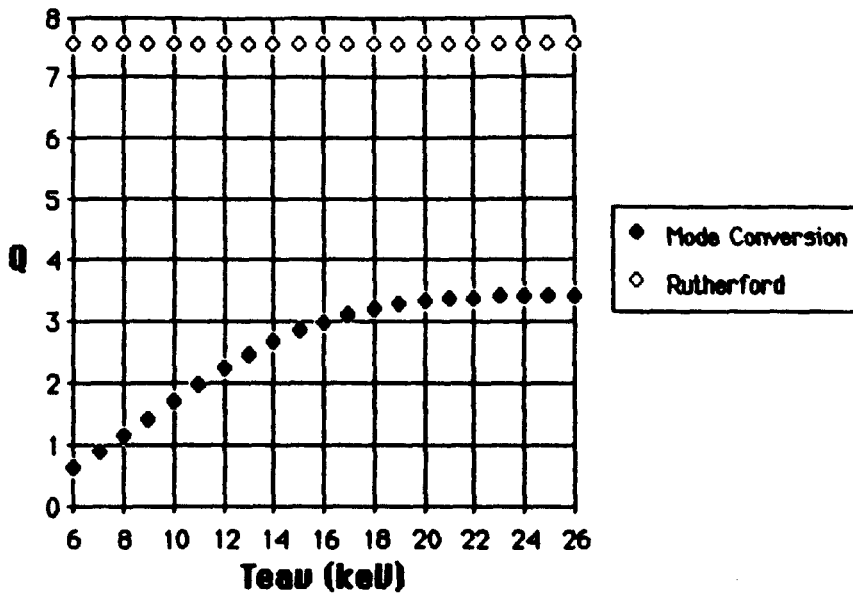


Figure 63

Slow Wave Lower Hybrid Q vs. Average Electron Temperature (keV)

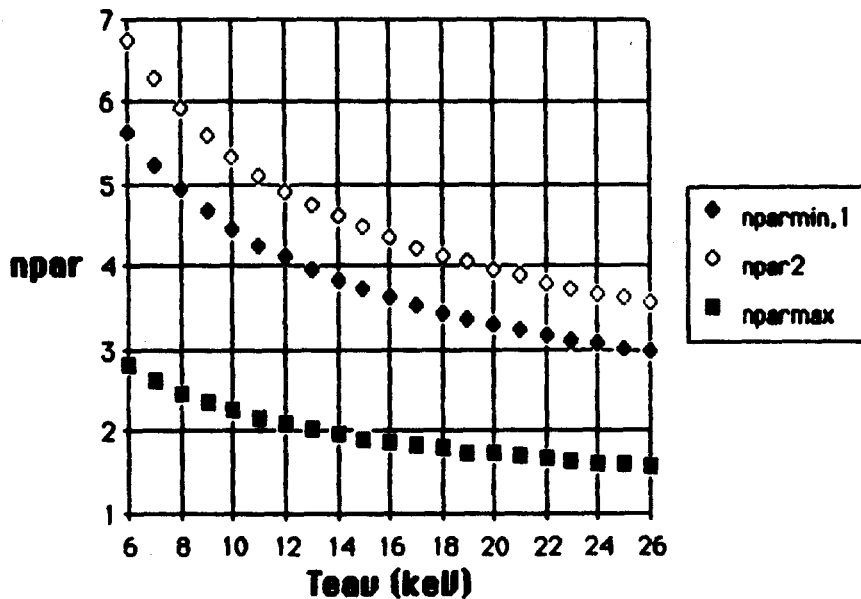


Figure 64

Parallel Indices of Refraction, Slow Wave vs. Average Electron Temperature (keV)